This is the peer-reviewed, final accepted version for American Mineralogist, published by the Mineralogical Society of America.
The published version is subject to change. Cite as Authors (Year) Title. American Mineralogist, in press.
DOI: https://doi.org/10.2138/am-2023-9021. http://www.minsocam.org/

Revision 2

The Olivine-Spinel-a^{melt}_{SiO2} (OSaS) Oxybarometer: A New Method for Evaluating Magmatic Oxygen Fugacity in Olivine-Phyric Basalts

Aaron S. Bell[1], Laura Waters[2], Mark Ghiorso[3]

[1]Department of Geological Sciences, University of Colorado Boulder, Boulder, CO 80309 USA
[2]Department of Earth and Environmental Science, New Mexico Institute of Mining and Technology, Socorro, NM 87801 USA [3] OFM Research

Abstract

The compositions of cotectic olivine-spinel pairs in mafic magmas provide information on the oxygen fugacity of their host liquid, which can be accessed with a thermodynamic analysis of the olivine-spinel-liquid peritectic reaction:

$$3Fe_2SiO_4^{oliv} + O_2^{sys} = 2Fe_3O_4^{sp} + 3SiO_2^{melt}$$

The extraction of redox information from cotectic olivine-spinel pairs requires a well-defined silica activity value (a^{melt}_{SiO2}) for the melt of interest, as well as a method to calculate $a^{oliv}_{Fe_2SiO_4}$ and $a^{sp}_{Fe_3O_4}$ from chemical analyses of olivine and spinel, respectively. In this work, we develop a new olivine-spinel-a^{melt}_{SiO2} (OSaS) oxygen barometer that utilizes MELTS to obtain values of a^{melt}_{SiO2}, which are used with values $a^{oliv}_{Fe_2SiO_4}$ and $a^{sp}_{Fe_3O_4}$ determined from established solution models for olivine and spinel. We find that two implementations of the spinel-liquid peritectic equilibria can successfully generate magmatic oxygen fugacity values, (1) using a combination of mineral activity models from the literature (classical-OSaS) and a^{melt}_{SiO2} determined from MELTS, and (2) directly from chemical potentials obtained from MELTS, where a correction is added to the MELTS-derived chemical potentials for the magnetite component of the spinel (MELTS-OSaS). The two implementations of the OSaS were tested by using each model to recover the experimentally reported fO_2 values for a dataset consisting of 50 olivine-spinel-glass assemblages derived from 14 published experimental studies. This dataset was filtered to remove potential disequilibrium phase assemblages, experiments with failed redox buffers, and poor-quality EMP analyses. Data quality metrics for the dataset filtration included Fe-Mg partitioning between olivine and melt, Fe-Mg partitioning between olivine-spinel, and an examination of whether a^{melt}_{SiO2} values were consistent with the reported phase assemblages. The classical-OSaS implementations reproduced the fO_2 values reported from the experimental dataset with a standard error estimate (SEE) of ±0.39, root mean standard error (RMSE) of ±0.40 and average deviation of ±0.31. In testing the MELTS-OSaS model, we identified that the solution model for magnetite underpredicted the values of $a^{sp}_{Fe_3O_4}$; therefore, we used the 50 experiments to assign a

This is the peer-reviewed, final accepted version for American Mineralogist, published by the Mineralogical Society of America.
The published version is subject to change. Cite as Authors (Year) Title. American Mineralogist, in press.
DOI: https://doi.org/10.2138/am-2023-9021. http://www.minsocam.org/

correction to the MELTS-predicted chemical potentials of magnetite. We tested the MELTS-OSaS model with the magnetite correction on a dataset of 18 additional buffered experiments, filtered for redox equilibrium and not included in the original experimental dataset. We find that the MELTs-OSaS model, which includes the correction for the magnetite chemical potential, reproduces fO_2 values for the 18 experiments with an SEE of ±0.20, root mean standard error (RMSE) of ±0.23 and average deviation of ±0.18. The OSaS oxybarometer can return magmatic fO_2 values with a standard error of ± 0.20 to 0.39 log units, depending on the model selected, provided that the olivine-spinel cotectic temperature is known to an accuracy of ±25°C, the H_2O content of the melt can be estimated within ±1.5wt%, and that the crystallization pressure of the olivine-spinel pair is < 500 MPa. We also propose that the OSaS models can be applied to experimental run products to determine or confirm oxygen fugacity values. We additionally suggest that the careful application of the OSaS oxybarometer can provide a reliable and robust alternative for performing redox studies on samples that do not contain sufficient glassy material to support the application of spectroscopic techniques (i.e., XANES and Mössbauer).

1. Introduction

Oxygen fugacity (fO_2) exerts critical influence on a wide range of petrologic and geochemical processes. In the broadest sense, oxygen fugacity plays a deterministic role in dictating the distribution of polyvalent elements (e.g., Fe, S, V, Mo, Cr) among various geochemical reservoirs - core, mantle, and crust - within the Earth (Arculus, 1979; Frost & McCammon, 2008). The bulk composition and speciation of magmatic fluids, which are ultimately emitted as fumarolic gasses (Gaillard & Scaillet, 2014; Moussallam et al., 2016; Ortenzi et al., 2020), are also directly controlled by magmatic oxygen fugacity; as such the prevailing fO_2 of planetary scale magma oceans exerts significant influence over the development and evolution of early planetary atmospheres (Deng et al., 2020; Hirschmann, 2012; Sossi et al., 2020). The influence of oxygen fugacity even extends to rheological properties of mantle peridotites, where it controls the point defect density in olivine and therefore its effective viscosity and seismic properties (Bai et al., 1991; Cline et al., 2018). Understanding the prevailing oxidation state of basaltic magmas underpins our ability to interpret and predict liquid-crystal phase equilibria along their liquid lines of descent, as well as the speciation and degassing behaviors of their dissolved C-H-S-O volatile components (Gaillard & Scaillet, 2014). Perhaps even more importantly, the fO_2 record preserved in primitive basaltic magmas is an accessible, albeit indirect, archive of redox heterogeneity among various geochemical reservoirs within the Earth's upper mantle. Comparisons of the fO_2 values estimated for basalts with those of their peridotite sources (Birner et al., 2018; Carmichael, 1991; Cottrell et al., 2020; Stolper et al., 2020) show broad agreement, suggesting that basalts are indeed faithful recorders of the fO_2 of their mantle sources. Thus, fO_2

measurements from basalts may provide insights into spatial and temporal changes in the oxidation state of the mantle driven by the deep Earth oxygen cycle.

Magmatic redox conditions are typically assessed by either spectroscopic measurements or thermodynamic phase equilibrium approaches. If glassy materials are available (e.g., matrix glass or melt inclusions), Fe K-edge XANES (X-ray Absorption Near Edge Spectroscopy) (Berry et al., 2003; Cottrell & Kelley, 2011; O'Neill et al., 2018; Zhang et al., 2018)) or Mössbauer Spectroscopy measurements are commonly employed to quantify $Fe^{3+}/\Sigma Fe$ ratios in glasses (O'Neill et al., 2018; Zhang, 2019). Measured $Fe^{3+}/\Sigma Fe$ ratios are subsequently converted into to oxygen fugacities using an established model that relates fO_2 to intensive variables such as temperature, pressure, and liquid composition (Jayasuriya et al., 2004; Kress & Carmichael, 1991; O'Neill et al., 2018; Borisov et al. 2018). Although basalt is one of the most abundant terrestrial, martian, and asteroidal materials, there are surprisingly few methods for appraising the magmatic oxygen fugacity of primitive samples lacking the glassy material required for the application of spectroscopic techniques.

Phase equilibrium-based approaches, such as the magnetite-ilmenite geothermometer and oxybarometer (Buddington & Lindsley, 1964; Ghiorso & Evans, 2008) or the olivine-orthopyroxene-spinel oxybarometer (Bryndzia and Wood 1990; Ballhaus et al., 1991), can in some instances be applied to samples not amenable to spectroscopic methods of study. Though phase equilibrium-based oxybarometers can partially fill the technique gap for holocrystalline samples, we stress that the existing methods are not without drawbacks and limitations. For example, the reliability of redox calculations from magnetite-ilmenite pairs is often compromised in mafic samples, as these phases are highly prone to kinetic disequilibrium during crystallization, insidious low temperature re-equilibration, and post-crystallization oxy-exsolution (Hou et al., 2020, and refs within). Furthermore, magnetite-ilmenite pairs commonly appear relatively late in the crystallization sequence of basaltic magmas, therefore they may reveal little about the oxidation state of more primitive liquids. The olivine-spinel-orthopyroxene equilibrium that was originally developed as an oxybarometer for spinel peridotites by Ballhaus et al. (1991) can also be adapted for use in basalts. However, many silica-undersaturated rocks (e.g., alkaline basalts and picrites) either do not become saturated with orthopyroxene late in the crystallization sequence or fail to crystallize orthopyroxene entirely, as in the case of critically silica undersaturated compositions (Carmichael et al., 1970). The dearth of mafic compositions that generate phase assemblages with usable orthopyroxene phenocrysts limits the application of the Ballhaus et al. (1991) oxygen barometer to bulk compositions that have silica activities sufficient to support orthopyroxene crystallization.

The development of new, user-friendly oxybarometers for compositionally diverse basalts is a critical step if magmatic redox studies are to be expanded to a wider range of samples and tectonic settings. We stress that basalts from tectonic settings (i.e., continental rifts) that generate relatively few rapidly

This is the peer-reviewed, final accepted version for American Mineralogist, published by the Mineralogical Society of America.
The published version is subject to change. Cite as Authors (Year) Title. American Mineralogist, in press.
DOI: https://doi.org/10.2138/am-2023-9021. http://www.minsocam.org/

quenched, glassy samples remain chronically understudied. In this work, we leverage thermodynamic calculations from the MELTS thermodynamic model collection (Ghiorso & Gualda, 2015; Ghiorso & Sack, 1995; Gualda et al., 2012) as implemented by the ThermoEngine Python Package (Thermoengine, 2022), hereafter referred to as MELTS, to develop two novel implementations of an oxybarometer that exploit the olivine-spinel-melt equilibria. A python code containing the model with both implementations and benchmark files are provided as part of the supplemental material (Appendix A1).

2. The Olivine-Spinel-a_{SiO2}^{melt} (OSaS) Equilibrium

Phase equilibrium experiments and the presence of ubiquitous octahedral Cr-spinel inclusions in Mg-rich olivine phenocrysts provide strong evidence that olivine and Cr-rich spinel are the first two phases that appear on the liquidus of primitive basaltic magmas (Médard & Grove, 2008; Roeder et al., 2006). As such, cotectic olivine-spinel pairs are uniquely suited to provide insights into the prevailing magmatic oxygen fugacity of primitive basaltic liquids. Using a reaction reminiscent of the olivine-spinel-orthopyroxene equilibrium developed by Ballhaus et al. (1991), the compositions of olivine and Fe^{3+}-bearing spinel can be formally connected to magmatic fO_2 through the peritectic reaction:

Eq.1 $$3Fe_2SiO_4^{oliv} + O_2^{sys} = 2Fe_3O_4^{sp} + 3SiO_2^{melt}$$

This reaction can be reformulated in thermodynamic notation to express oxygen fugacity as a function of the activity of the fayalite component of olivine ($a_{Fe_2SiO_4}^{oliv}$), the activity of the magnetite component of the spinel ($a_{Fe_3O_4}^{sp}$), and the activity of SiO_2 in the melt (a_{SiO2}^{melt}):

Eq. 2 $$\log_{10} fO_2 = \frac{-\Delta G^\circ_{T,P}}{\ln(10)RT} + 3\log a_{SiO_2}^{melt} + 2\log a_{Fe_3O_4}^{sp} - 3\log a_{Fe_2SiO_4}^{oliv}$$

Provided that the crystallization temperature for an olivine-spinel pair is known, the application of Eq. 2 to evaluate magmatic fO_2 simply requires one to obtain values for $\Delta_r G^\circ_{(T,P)}$, $a_{Fe_2SiO_4}^{oliv}$, $a_{Fe_3O_4}^{sp}$, and a_{SiO2}^{melt}. The calculation of $\Delta_r G^\circ_{(T,P)}$, $a_{Fe_2SiO_4}^{oliv}$, and $a_{Fe_3O_4}^{sp}$ is a relatively straightforward exercise, as standard state thermodynamic data (e.g., $\Delta_f H_{Tr}$, S°_{Tr}, heat capacity functions, and molar volumes for the phases of interest) as well as solution models for the crystalline phases of interest are readily available. Obtaining a_{SiO2}^{melt} values for basaltic melts that are compatible with Eq. 2 is a more difficult prospect, as the potential methods for obtaining this value are either insufficiently accurate or remain untested with respect to their efficacy when applied to fO_2 calculations.

This is the peer-reviewed, final accepted version for American Mineralogist, published by the Mineralogical Society of America.
The published version is subject to change. Cite as Authors (Year) Title. American Mineralogist, in press.
DOI: https://doi.org/10.2138/am-2023-9021. http://www.minsocam.org/

2.1 The Trouble with Calculating a_{SiO2}^{melt} in from Mineral-Melt Equilibria

One approach for obtaining the a_{SiO2}^{melt} values for silicate magmas employs mineral-melt equilibria, such as the olivine-orthopyroxene-melt peritectic reaction. Though this approach presents the simplest solution for calculating a_{SiO2}^{melt}, we note that equilibrium orthopyroxene-olivine pairs are relatively rare in primitive tholeiites that crystallize at shallow crustal pressures. Furthermore, orthopyroxene is entirely absent in critically silica-undersaturated alkali basalts and basanites (Carmichael et al., 1970). It is possible to reformulate the olivine-orthopyroxene-melt equilibrium in which the activity of the clinoenstatite component (augite) is substituted for the activity of enstatite in orthopyroxene. The peritectic reaction between olivine, the clinoenstatite component of high-Ca pyroxene (augite) and the melt offers an alternative approach for obtaining a_{SiO2}^{melt} for basaltic phase assemblages that lack orthopyroxene. In magmas co-saturated with olivine and clinopyroxene the a_{SiO2}^{melt} can be defined with the equilibrium:

Eq. 3 $$Mg_2SiO_4^{oliv} + SiO_2^{melt} = 2MgSiO_3^{clinoenst}$$

which can be re-arranged as:

Eq. 4 $$\log a_{SiO2}^{melt} = \frac{-\Delta G°_{T,P}}{\ln(10)RT} + 2\log a_{MgSiO3}^{cpx\ or\ opx} - \log a_{Mg2SiO4}^{oliv}$$

The $\Delta_r G°_{(T,P)}$ that appears in Eq. 4 is calculated from the standard state thermodynamic properties of clinoenstatite, rather than orthoenstatite. On the surface, this approach offers an appealing solution to the a_{SiO2}^{melt} problem, however there are several notable issues which diminish the effectiveness of this approach. The first issue is that cotectic olivine-spinel pairs may not be in equilibrium with augite phenocrysts in the assemblage, as clinopyroxene often appears relatively late in the crystallization sequence for melts experiencing low crystallization pressures (e.g., Sisson and Grove, 1993). The second issue is that the efficacy of this method largely depends on how well the selected clinopyroxene solution model performs for the composition of interest. For example, Bucholz and Keleman (2019) explored this approach and applied it to a suite of deep-crustal, ultramafic basaltic cumulates to determine a_{SiO2}^{melt}. They demonstrate that a_{SiO2}^{melt} values calculated in this manner critically depend on the pyroxene solution model's ability to generate accurate a_{MgSiO3}^{cpx} values. The results of Bucholz and Keleman (2019) underscore the difficulty of using a_{MgSiO3}^{cpx} values predicted for high Ca-enriched clinopyroxene. The a_{MgSiO3}^{cpx} for Ca-enriched clinopyroxenes are insufficiently accurate for performing redox calculations, as the a_{SiO2}^{melt} values for these

compositions are consistently underpredicted, which in turn, systematically skews the resultant fO_2 towards values that are too reduced.

Nikolaev et al. (2016) also attempted to exploit the olivine-spinel-melt equilibria to formulate an empirical oxybarometer for magmatic phase assemblages containing cotectic olivine-spinel pairs. In this approach the authors adopted a formulation which does not explicitly account for silica activity, where oxygen fugacity was cast as an empirical function of olivine composition, spinel composition, and temperature. Though this model successfully returns fO_2 values for many compositions, we stress that that the value assumed by a_{SiO2}^{melt} in many cases exerts significant leverage on the resultant fO_2. As such, empirical models lacking terms accounting for the impact of a_{SiO2}^{melt} (which we note is not only a function of liquid composition, but also a function of pressure and dissolved water content) cannot serve as a universal model for all magmatic systems, and may produce systematically biased results for systems that have a_{SiO2}^{melt} dissimilar to the coarse "average" a_{SiO2}^{melt} inherent to the calibration dataset.

3. Using MELTS to Obtain a_{SiO2}^{melt} for the OSaS Oxybarometer

In the absence of a silica activity buffering phase assemblage, MELTS may be utilized to obtain the silica activity for the liquid of interest through calculations of the chemical potential of silica (μ_{SiO2}^{melt}) for multi-component silicate melts. The μ_{SiO2}^{melt} values calculated from the MELTS algorithm can be converted into activity values using the expression:

Eq. 5 $$\mu_{SiO2}^{melt} - \mu^{\circ}_{SiO2} = RT(\ln a_{SiO2}^{melt})$$

where μ_{SiO2}^{melt} is the chemical potential of the SiO_2 component of the melt obtained from MELTS and μ°_{SiO2} represents the standard state chemical potential to which the a_{SiO2}^{melt} value is being referenced. The value of μ°_{SiO2} can refer to either the chemical potential of pure liquid SiO_2 or the chemical potential of one of several crystalline SiO_2 polymorphs. All calculations of μ_{SiO2}^{melt} performed in this work utilized the Rhyolite MELTS models of Ghiorso and Gualda (2015); the μ_{SiO2}^{melt} values were subsequently converted into obtaining a_{SiO2}^{melt} values for the liquid of interest.

Using MELTS, one can readily obtain a_{SiO2}^{melt} for a basaltic melt composition of interest and subsequently insert that value along with appropriate values of $a_{Fe_2SiO_4}^{oliv}$ and $a_{Fe_3O_4}^{sp}$ into Eq.2 to calculate fO_2. This approach is appealing for its familiar form (Eq. 2) and relative simplicity; for this reason, we hereafter refer to this approach as the "classical-OSaS oxybarometer." In this version of the OSaS oxybarometer, we have opted to calculate $\Delta_r G^{\circ}_{(T,P)}$ for the OSaS equilibrium with the internally consistent thermodynamic

This is the peer-reviewed, final accepted version for American Mineralogist, published by the Mineralogical Society of America.
The published version is subject to change. Cite as Authors (Year) Title. American Mineralogist, in press.
DOI: https://doi.org/10.2138/am-2023-9021. http://www.minsocam.org/

dataset of Berman (1988), as it is inherently compatible with thermodynamic data generated from MELTS. The $\Delta_rG°_{(T,P)}$ values for Eq.1 were calculated using the standard state properties of crystalline SiO_2, rather than pure silica liquid, therefore the a_{SiO2}^{melt} values obtained from MELTS reference a high temperature polymorph of quartz as the standard state. We also note that it is possible to calculate $\Delta_rG°_{(T,P)}$ values for the OSaS oxybarometer using the Holland and Powell (2011) thermodynamic database. The $\Delta_rG°_{(T,P)}$ values calculated from the Berman (1988) and the Holland and Powell (2011) datasets differ by less than 1.5 kJ mol^{-1} (from 1100°C to 1300°C). The subtle differences in the $\Delta_rG°_{(T,P)}$ obtained from the two databases translates to a difference in oxygen fugacity values of < 0.075 log units for the end-member quartz-fayalite-magnetite buffer reaction. This comparison suggests that implementing $\Delta_rG°_{(T,P)}$ calculated from either the Berman (1988) or the Holland and Powell (2011) databases in the OSaS should return nearly identical fO_2 values.

We use the olivine solution model of O'Neill et al. (2003) to calculate fayalite activities, as the interaction parameter from this model is consistent with the calorimetrically determined mixing parameters of Dachs and Gieger (2007). Using the symmetric regular solution model of O'Neill et al. (2003), fayalite activity is calculated, using Eqs. 6 & 7:

Eq. 6 $$RT\ln\gamma_{Fe2SiO4}^{oliv} = X_{Mg_2SiO_4}^2 W_{Fe\text{-}Mg}^{oliv}$$

Eq. 7 $$a_{Fe_2SiO_4}^{oliv} = \left[X_{Fe_2SiO_4}\gamma_{Fe_2SiO_4}^{oliv}\right]^2$$

Where R is the universal gas constant, T is the temperature in K, and $W_{Fe\text{-}Mg}^{oliv}$ is the binary interaction parameter that assumes a value of 2.3 kJ mol^{-1}. The activity of the magnetite component of the spinel was calculated using the solution model of Nell and Wood (1990) which was given in an empirical form by Wood (1991) as:

Eq. 8 $$\log a_{Fe_3O_4}^{sp} = \left(\frac{(Fe^{2+})(Fe^{3+})}{4}\right)^2 + \frac{1}{T}\left[406(Al)^2 + 653(Mg)(Al) + 299(Cr)^2 + 199(Cr)(Al) + 463(Mg)(Cr)\right]$$

where the element in parenthesis refers to the number of cations present per spinel formula unit normalized to four oxygen anions. Ferric and ferrous ratios and cation site occupancy calculations follow the procedure of the SPINCALC spreadsheet (found at http://www.gabbrosoft.org); the SPINCALC charge balance and normalization procedure is implemented into the python code and applied to the classical OSaS.

In addition to the classical-OSaS method described above, the MELTS algorithm can also be applied to the olivine-spinel-a_{SiO2}^{melt} equilibrium in a slightly different, though more fundamental way. Rather

than using MELTS to obtain a_{SiO2}^{melt} values for use in Eq. 2, MELTS can alternatively be used in a second implementation of Eq. 2 to directly calculate the chemical potentials of the fayalite endmember in the olivine solution of interest, the magnetite endmember of spinel solution of interest, and SiO_2 in the melt of interest. This approach has the advantage of using the internally consistent solution models and thermodynamic dataset intrinsic to the MELTS software. Chemical potentials calculated from MELTS can be arranged to define fO_2 as follows:

Eq. 9 $$\mu_{O2}^{sys} = 3\mu_{SiO2}^{melt} + 2\mu_{Fe3O4}^{sp} - 3\mu_{Fe2SiO4}^{oliv}$$

where the chemical potential μ_{O2}^{sys} obtained from Eq.5 can be converted into oxygen fugacity, using the standard state thermodynamic data for O_2 reported in the JANAF tables (Chase, 1998), as in Eq. 10:

Eq. 10 $$\mu_{O2}^{sys} - \mu^{\circ}_{O2} = RT\ln fO_2$$

The "MELTS-only" version oxybarometer described above (hereafter referred to as the MELTS-OSaS oxybarometer) has the advantage of using solution models and a thermodynamic data set that are internally consistent. As such, the solution models for olivine and spinel endemic to this approach are different than the models implemented in the previous form of the classical-OSaS oxybarometer. MELTS calculations employ the Sack and Ghiorso (1989) olivine solution model for the calculation of $\mu_{Fe2SiO4}^{oliv}$ and the Sack and Ghiorso (1991) spinel solution model for the calculation of μ_{Fe3O4}^{sp}.

4. Evaluating the OSaS Oxybarometers: Calculating the Oxygen Fugacity Recorded by Olivine-Spinel-Glass Sets in Redox Controlled Phase Equilibrium Experiments

Although the two versions of the OSaS oxybarometer described above should in principle generate accurate magmatic oxygen fugacity data for equilibrium olivine-spinel pairs, we stress that both approaches still require a rigorous test before being applied to 'real world' magmatic redox studies. The primary objective of this work is to develop a working oxybarometer that can be applied to cotectic olivine-spinel (±glass) assemblages in holocrystalline basalts that lack phase assemblages amenable to other established oxybarometers. To assess the efficacy of each of the approaches, we apply each method to a suite of redox buffered phase equilibrium experiments drawn from the literature. We used the Library for Experimental Phase Relations (LEPR) (Hirschmann et al., 2008) and conducted a literature search to identify an initial set of validation experiments which (1) contained olivine-spinel-liquid phase assemblages and (2) were conducted at controlled fO_2. In total, we identified 223 experiments from 33 experimental studies. The bulk

This is the peer-reviewed, final accepted version for American Mineralogist, published by the Mineralogical Society of America.
The published version is subject to change. Cite as Authors (Year) Title. American Mineralogist, in press.
DOI: https://doi.org/10.2138/am-2023-9021. http://www.minsocam.org/

compositions of the starting materials used in these experiments range in composition from alkaline to subalkaline and from mafic to intermediate.

4.1 Filtering Experimental Dataset

From this initial dataset we omit experiments with spinel analyses that contain >0.7 wt% SiO_2 to reduce any interference of groundmass glass contamination for calculation of spinel component activities. We also filtered the for experiments that contained olivine-melt pairs with $K_d^{\text{oliv-melt}}_{\text{Fe-Mg}}$ values consistent with the attainment of equilibrium. For melt compositions low in total alkali content, we only selected experiments in which $K_d^{\text{ol-melt}}_{\text{Fe-Mg}}$ values vary between 0.30±0.08 (Fig. 1A). Lower $K_d^{\text{ol-melt}}_{\text{Fe-Mg}}$ values were accepted for melts that contained higher concentrations of alkalis (Fig. 1A), as it has been shown that increasing alkali content and decreasing silica activity effectively depress $K_d^{\text{oliv-melt}}_{\text{Fe-Mg}}$ values (Toplis, 2005). We intentionally employ a wide filter for the olivine $K_d^{\text{oliv-melt}}_{\text{Fe-Mg}}$ values, as our goal is to test the oxygen barometers across a spectrum of liquid compositions with variable silica activities.

We also evaluated experiments for the attainment of equilibrium between spinel and olivine. Depending on the choice of experimental starting material, it is possible for experiments to inherit relict spinel crystals that are out of equilibrium with the olivine and liquid present in the experiment. Disequilibrium or un-melted spinel crystals may remain in experimental phase assemblages because of sluggish re-equilibration kinetics or short experimental run times, which may be required to maintain a viable redox buffer assemblage. We use an empirical approach to filter out experiments that contain disequilibrium spinel. The distribution of Fe^{2+} and Mg between olivine and spinel can be described with the exchange equilibrium:

Eq. 11 $$X_{Mg}^{ol} + X_{Fe2+}^{sp} = X_{Fe2+}^{ol} + X_{Mg}^{sp}$$

Unlike olivine, a single canonical Fe-Mg exchange coefficient cannot be ascribed to olivine-spinel pairs. We found that within the experimental dataset, the Fe^{2+}-Mg exchange coefficient depends primarily on the Al-content of the spinel (Fig. 1B). We also examined the dataset for a potential relationship between $K_d^{\text{ol-sp}}_{\text{Fe}^{2+}\text{-Mg}}$ and Cr content of the spinel, however, we found no significant correlation. The calculated $K_d^{\text{ol-sp}}_{\text{Fe}^{2+}\text{-Mg}}$ values increase with increasing Al content (Fig. 1B) for the dataset and fall on a linear trend described by:

Eq. 12 $$K_D^{\text{ol-sp}}_{\text{Fe}^{2+}\text{-Mg}} = 0.249X_{Al} + 0.034$$

This is the peer-reviewed, final accepted version for American Mineralogist, published by the Mineralogical Society of America.
The published version is subject to change. Cite as Authors (Year) Title. American Mineralogist, in press.
DOI: https://doi.org/10.2138/am-2023-9021. http://www.minsocam.org/

Where X_{Al} is the number of Al cations per spinel formula unit (normalized to four oxygen anions). The observed relationship between $K_d\,{}^{\text{ol-sp}}_{Fe^{2+}\text{-Mg}}$ and the identity of the dominate cation occupying the octahedral site (Al^{3+}, Cr^{3+}, or Fe^{3+}) in the spinel is consistent with the reciprocal solution behavior exhibited by spinel (Wood and Nicholls 1978), as well as the results of previous studies of olivine-spinel partitioning (Evans and Frost, 1975). The linear trend described by Eq. 12 may be thought of as an apparent equilibrium trend, and as such is a useful tool for evaluating whether a given olivine-spinel pair represents an equilibrium assemblage. Using this criterion, we discarded eleven experiments that contained olivine-spinel pairs that plotted off the apparent equilibrium K_D trend (±0.1). We show the linear fit of the initial and filtered dataset in Fig. 1B to highlight the minimal change imparted to the fit after removing disequilibrium spinels.

Accurate control of oxygen fugacity is a fundamentally challenging problem in experimental petrology (Grove, 1981). Reported oxygen fugacity values from 1-bar gas mixing experiments are typically accurate, as they can be directly assessed with yttrium- or calcium-stabilized zirconia oxygen sensors. However, higher pressure experiments that rely on double capsule techniques that employ solid mineral redox buffer assemblages may either fail to achieve redox equilibrium or fail to maintain redox equilibrium over the duration of the experiment. It is difficult to assess the quality of literature-reported fO_2 values or their affiliated uncertainties (if reported), however, we have attempted to identify experiments from the dataset that likely failed to attain or maintain redox equilibrium using a simple test based on calculated values of a_{SiO2}^{melt}. In this "reasonableness" test, we initially assume that each experiment was buffered at the reported fO_2, and then we solve for the a_{SiO2}^{melt} using a rearranged form of Eq. 2 (Fig. 1C). We find that a_{SiO2}^{melt} values generated for many experiments plot in petrologically unreasonable regions of temperature-a_{SiO2}^{melt} space. We identified experiments where $\log_{10}a_{SiO2}^{melt} < 0.25$ or $\log_{10}a_{SiO2}^{melt} > 0.75$ as being suspicious, as the phase assemblages in these experiments are inconsistent with such extreme silica activity values. For example, experiments that return $\log_{10}a_{SiO2}^{melt}$ values > 0.75 (~$\log_{10}a_{SiO2}^{melt} = -0.15$) should contain orthopyroxene as a liquidus phase instead of olivine (Fig. 1C) and other samples that plot above $\log_{10}a_{SiO2}^{melt}=1$ should be saturated with a crystalline SiO_2 polymorph which is inherently incompatible with the presence of olivine phenocrysts. Likewise, experiments that have $\log_{10}a_{SiO2}^{melt}$ values < 0.25 (~$\log_{10}a_{SiO2}^{melt} = -0.60$) plot below perovskite-sphene silica buffer curve in the stability field of feldspathoid group minerals. Rare terrestrial rocks such as olivine melilites and extraterrestrial basalts (such as angrite meteorites) may have $\log_{10}a_{SiO2}^{melt}<0.25$, however, the bulk compositions of the experiments considered for the calibration dataset bear no resemblance to these exotic compositions. The silica activity test allows us to directly assesses consistency of a_{SiO2}^{melt} values constrained by thermodynamic analysis of *independent* peritectic reactions. The presence or absence of orthopyroxene, quartz, or nepheline in the experimental phase assemblages

effectively constrains the range of permissible silica activity values vis a vis the pertinent a_{SiO2}^{melt} buffer reactions. In other words, this test is effectively a comparison of a_{SiO2}^{melt} values calculated with the OSaS reaction to a_{SiO2}^{melt} constraints from other mineral-melt reactions that define silica activity. We emphasize that experiments are not excluded on their a_{SiO2}^{melt} value alone. Rather, this test excludes experiments that have a_{SiO2}^{melt} values that are inconsistent with reported phase assemblage of the experimental charge in question. For example, an experimental melt that does not contain quartz cannot have an $\log_{10} a_{SiO2}^{melt} > 1.0$. The extreme high and low a_{SiO2}^{melt} values obtained for the experimental melts may be attributed to several factors, including: (1) inaccurate spinel analyses, (2) unrecognized compositional zoning in olivine, or (3) a failed redox buffer assemblage. We omit these experiments from our calibration dataset, as some component of the olivine-spinel-a_{SiO2}^{melt}-fO_2 system reflects disequilibrium, where the mineral assemblage reported in the run products is inconsistent with the mineral assemblage predicted by the calculated values of a_{SiO2}^{melt}. After culling the experimental dataset using the olivine-spinel Fe^{2+}-Mg exchange coefficient test and the a_{SiO2}^{melt} "reasonableness" test, our final dataset consists of 50 experiments on natural liquids.

In total, 19 experiments failed the olivine and liquid ${}^{Fe\text{-}Mg}K_D$ test; of those 19 experiments two experiments also failed the test of olivine-spinel equilibrium, and 11 also failed the a_{SiO2}^{melt} test. Eleven experiments failed the test of olivine-spinel equilibrium, where two of the 11 experiments also failed the olivine and liquid ${}^{Fe\text{-}Mg}K_D$ test and one of the 11 experiments failed the a_{SiO2}^{melt} test. Finally, 91 experiments failed the a_{SiO2}^{melt} test, meaning that their calculated values of a_{SiO2}^{melt} suggest that the experiments should be saturated in feldspathoids, orthopyroxene or quartz, but neither of these phases are reported in the run products. A single experiment failed all three tests. We note that all olivine-spinel pairs in our culled dataset are also consistent (within±0.1) with the olivine-spinel equilibrium proposed by Li et al. (1995), which accounts for variations in temperature. The final data set includes liquid compositions that range from basanite to andesite (Fig. 2) (Supplemental Data Table S1).

4.2 Evaluating the Performance of the Classical OSaS Oxybarometer

We used the activities of olivine and spinel, and the a_{SiO2}^{melt} values relative to tridymite (using Eq. 5) for the experimental glasses and the $\Delta_r G°$ values based on the Berman (1988) database to solve for fO_2 based on Eq. 2. We find that this approach generates fO_2 values for the experiments in the initial validation dataset with an RMSE of ± 0.40 log units, a standard error estimate of ±0.39 log units and an average residual (the average of the absolute values of the residual for each experiment) of ±0.31 log units (Fig. 3A). We find a few weak patterns in the residuals of the OSaS oxybarometer (Fig. 4), however, all the residual slopes appear to be negligible within the average residual of the model. The greatest trend is associated with H_2O content, which cannot be deconvolved from pressure in experiments in the test dataset.

This is the peer-reviewed, final accepted version for American Mineralogist, published by the Mineralogical Society of America.
The published version is subject to change. Cite as Authors (Year) Title. American Mineralogist, in press.
DOI: https://doi.org/10.2138/am-2023-9021. http://www.minsocam.org/

For melts from experiments conducted at high water contents and high pressures, the model systematically underestimates the reported fO_2 values (Fig. 4C). We also find there is a weak correlation between the fO_2 residual and both melt and olivine compositions, such that the model systematically underestimates fO_2 for silica-rich liquids and forsterite-rich olivine (e.g., Fo_{90}; Fig. 4D), however, we stress that these correlations are weak and are smaller in magnitude than the average residual of the model. We suggest that the classical OSaS model should not be applied to olivine-spinel-glass assemblages with melts that contain more than 10 wt.% H_2O.

4.3 Evaluating the Performance of the MELTS-OSaS Oxybarometer

We used the MELTs algorithm to calculate the chemical potentials of spinel, olivine, and SiO_2 in the melt using compositions, temperatures, and pressures reported for the experiments included in the culled evaluation dataset. The resultant chemical potentials were inserted into Eq. 9 to obtain μO_2, which we then converted into an fO_2 using Eq. 10. The MELTS-OSaS approach reproduces fO_2 values of the initial validation dataset with an average residual of +0.76 log units. The MELTS-OSaS approach systematically underpredicts the fO_2 of experiments with equilibrium spinel compositions that are enriched in chromium and aluminum (Fig. 5).

This result suggests that we have identified an equilibrium for which the internally consistent MELTS model does not reproduce the experimental data with an acceptable margin of error. At the most fundamental level, the mismatch between the experimental and predicted fO_2 values is reflected by a deficit chemical potential calculated for the reaction of interest (Eq. 9). There are two potential sources of this deficit (1) the standard state μ° values used for any of the end-member phases or (2) the chemical potential associated with the excess mixing properties derived from the solution model of choice (we also stress that these two possibilities are not mutually exclusive). Given the internal consistency of the Berman thermodynamic dataset that underpins the MELTS OSaS and the fact that it faithfully reproduces experimentally determined equilibrium fO_2 values of the fayalite-magnetite-quartz buffer, there is no evidence implicating the standard state properties as the source of the observed error. Therefore, it is likely that the source of the error is related to the mixing properties defined by either the olivine or spinel solution model.

4.3.1 Source of the energy deficit in the MELTS OSaS equilibrium: olivine or spinel?

The observed MELTS OSaS chemical potential deficit can potentially be attributed to deficiencies values of μ^{sp}_{Fe3O4} or $\mu^{oliv}_{Fe2SiO4}$ predicted by the spinel and olivine solution models, respectively. We evaluate which phase is the source of the energy deficit by comparing the residuals from the MELTS OSaS model (known-predicted values of $\log fO_2$) as a function of the compositions of olivine and spinel (Fig. 6). We find that the residuals from the MELTS OSaS show the strongest correlations with the composition of the

spinel, in particular the Cr-content and Cr# (residuals vs. Cr# yield $R^2 = 0.45$, p-value= 9.8×10^{-8}; Fig. 6A), where the lowest residuals coincide with spinel compositions with low concentrations of Cr. Furthermore, we find that the average residual for the nine experiments that have spinel compositions with Cr#<0.01 is +0.24 log units which suggests that the MELTS OSaS model performs well for spinel compositions that are effectively binary $MgAl_2O_4$-Fe_3O_4 or Fe_2TiO_4-Fe_3O_4 mixtures. In contrast, residuals show a much weaker correlation with olivine composition (residuals vs. mol% fayalite yields $R^2 = 0.15$, which is reduced to 0.07 if a single, fayalite-rich olivine at the far right-hand side of the fit is discarded; Fig. 6B). We also note that when the Sack and Ghiorso (1989) solution model is used in the internally consistent MELTS architecture, it has been demonstrated that it successfully reproduces a preponderance of the experimental phase equilibrium data on which it was evaluated. The broad success of the Sack and Ghiorso (1989) olivine solution model within the MELTS architecture is a strong argument that the observed chemical potential deficit is not, in fact, related to a mishandling of the olivine solution properties.

The observed correlations between spinel composition and residuals suggest Cr parameterization of Sack and Ghiorso (1991b) - which was meant to extend to the original Sack and Ghiorso (1991a) model for Fe-Mg-titanomagnetite-aluminate spinel to Cr-bearing compositions - underpredicts magnetite activity for spinel compositions that contain a chromite component. We emphasize that composition space for spinel is large and that the solution properties of spinel are exceedingly complicated. The configurational entropy of normal-inverse spinel solutions is impacted by temperature-dependent ordering on the cation sublattice; therefore, spinel solution models contain provisions to predict configurational entropy for a given composition. Magnetite activity values are influenced solution model implicit parameters that account for compositionally driven variations in cation distributions (i.e., the inversion parameter and its temperature dependence). Kurepin (2005) re-evaluated degree of inversion and cation mixing across the chromite-magnetite binary with new lattice parameter data and found that the Sack and Ghiorso (1991b) Cr extension overestimates the inversion parameter for Cr bearing compositions. The Kurepin (2005) work suggests that that the inversion parameter is nearly zero for spinel that contain dilute magnetite concentrations (i.e., < 25 mol. % Fe_3O_4). If this is correct, then the overestimation of the inversion parameter results in configurational entropy estimates that are too high, which would translate to $a^{sp}_{Fe_3O_4}$ values that are too low. The use of low $a^{sp}_{Fe_3O_4}$ in OSaS equilibrium will, by extension generate fO_2 values that are also too low, which is consistent with the observed behavior of the residuals for experiments that contain Cr spinel.

4.3.2 Correction to μFe_3O_4 values

We developed an empirical correction that can be applied to the μFe_3O_4 values generated by MELTS. This correction effectively increases the MELTS-derived μFe_3O_4 values to bring them into

This is the peer-reviewed, final accepted version for American Mineralogist, published by the Mineralogical Society of America.
The published version is subject to change. Cite as Authors (Year) Title. American Mineralogist, in press.
DOI: https://doi.org/10.2138/am-2023-9021. http://www.minsocam.org/

equilibrium with the reported fO_2 values for the experiments in the initial validation dataset. The equilibrium values for μFe_3O_4 (i.e., $\mu_{Fe3O4}^{spinel-eq}$ in Eq. 13 below) can be obtained by rearranging Eq. 9 such that:

Eq.13 $$\mu_{Fe3O4}^{spinel\text{-}eq} = -(3\mu_{SiO2}^{melt} - 3\mu_{Fe2SiO4}^{olivine} - \mu_{O2})/2$$

We conducted a multivariate linear regression to relate the difference in the equilibrium μ_{Fe3O4}^{spinel} values ($\mu_{Fe3O4}^{spinel-eq}$) and MELTS μ_{Fe3O4}^{spinel} values to the composition of the spinel (as mole fractions of oxide components). We systematically removed inconsequential compositional terms from the regression until we reached a combination of statistically significant terms and a low standard error on the regression fit. We find that the intercept, the initial, uncorrected value of μFe_3O_4 from MELTS, and a subset of oxide "components" (X_{Cr2O3}, X_{MgO}, X_{FeOT}) are all significant terms (p-values ≤0.02) (Table 1; Fig. 7A) and the model fit reproduces the idealized μFe_3O_4 values with a standard error estimate of ± 4.816 kJ, which is equivalent to an uncertainty of ± 0.17 log units of fO_2. Seven significant figures are required for each of the regression coefficients, as using less than the seven significant figures (i.e., rounding) will result in μFe_3O_4 that are insufficiently precise for calculating accurate fO_2 values. It is also important to note that the corrected equilibrium μFe_3O_4 values obtained through this regression cannot be reincorporated into the MELTS algorithm, as they are no longer internally consistent with supporting model parameters. Using the newly derived regression equation (Table 1) to calculate μFe_3O_4 from MELTS outputs, we find that the MELTS OSaS can successfully reproduce the fO_2 values for the experimental dataset with a SEE of ±0.35 log units. Additionally, we find no significant patterns in the residuals as a function of spinel composition (Fig. 7B).

To understand the error of the MELTS-OSaS oxygen barometer, we must apply it to experiments that were not used to calibrate the correction to μFe_3O_4. We identified an additional 18 experiments that were not either (1) not found during our initial, imperfect, search of the LEPR database and literature or (2) were published after the initial testing and calibration of the MELTS-OSaS oxybarometer (Supplemetal Table S2). This additional test dataset includes the experiments of Gaetani et al. (1994), Melekova et al. (2017), Takagi et al. (2005), Krawczynski et al. (2012) and Zhang et al. (2023). We have applied the MELTs-OSaS oxybarometer to predict the fO_2 values of these experiments and found that the MELTS-OSaS with a corrected μFe_3O_4 returns fO_2 values for most of these experiments with of ± 0.23 log units, a standard error estimate of ±0.20 log units and an average residual (the average of the absolute values of the residual for each experiment) of ±0.18 log units (Fig. 7C).

We additionally tested this model on experiments on picritic melts with >10 wt.% MgO from Matzen et al. (2011) and Zhang et al. (2023) (which pass all filters but were not included in either of the preceding experimental datasets; Supplemental Table S3). We found that both the MELTS-OSaS and the

This is the peer-reviewed, final accepted version for American Mineralogist, published by the Mineralogical Society of America.
The published version is subject to change. Cite as Authors (Year) Title. American Mineralogist, in press.
DOI: https://doi.org/10.2138/am-2023-9021. http://www.minsocam.org/

462 classical-OSaS models overestimate the fO_2 of picritic liquids by an average of +0.29 log units and by +0.42
463 log units, respectively (Supplemental Fig. S1). We observe that this effect is confined to liquid compositions
464 containing >10.0 wt. % MgO. This effect suggests that MELTS systematically overpredicts a_{SiO2}^{melt} values
465 for liquid compositions enriched in normative olivine, therefore, we caution users to be cognizant of the
466 small, albeit systematic, fO_2 bias imparted to MgO-rich liquids.
467 We find a few weak patterns in the residuals for the validation dataset (Fig. 8A-D), but the
468 magnitudes of the correlation slopes are negligible within the average residual of the model and lower in
469 magnitude than those of the classical OSaS oxybarometer for a given parameter. The model has some
470 pattern in residual with increasing SiO_2 concentration (Fig. 8A) and H_2O content (Fig. 8C) of the coexisting
471 melt, both of which impact the activity of silica parameter used in the model. Like the classical OSaS
472 oxybarometer, the residuals associated with the MELTs OSaS oxybarometer indicate that the model
473 satisfactorily reproduces the evaluation dataset. The model's performance is significantly degraded for
474 olivine-spinel-glass assemblages that grew from extremely H_2O rich melts (e.g., > 10 wt.%). Therefore, as
475 with the classical OSaS oxybarometer, we strongly caution against applying the MELTS OSaS model to
476 water-rich systems, as it may produce inaccurate results.
477 In general, the fO_2 values generated from the two models are in good agreement when considering
478 the error estimates of both models (Fig. 9). The mean difference in fO_2 predicted by the two models for the
479 18 experiments used to test the MELTS-OSaS barometer is –0.12 log units and the average absolute value
480 of the difference in the fO_2 predicted by the two models is 0.2 log units.
481
482 **5. Uncertainties and Limitations of the Classical and MELTS OSaS Oxybarometers**

483 The advantage to testing the classical-OSaS and MELTS-OSaS oxybarometers on experiments is
484 that they are conducted at known temperatures, pressures, and water contents. As the goal of this work is
485 to provide a method for estimating fO_2 in natural samples, we have also attempted to evaluate how well the
486 model performs when intensive and compositional variables are not well known. Temperature exerts a
487 principal control $\Delta_rG°$ values that appear in Eq. 2, as well as (though to a lesser extent) the mineral and melt
488 activities calculated from the solution models. Both OSaS formulations are mildly dependent on pressure
489 and the dissolved H_2O content of the liquid of interest. Like temperature, pressure also directly impacts Δ_rG
490 for the reaction of interest, as well as the a_{SiO2}^{melt} value calculated from MELTS. The dissolved water content
491 of the melt exerts considerable influence on the a_{SiO2}^{melt} (Carmichael 1970), where increasing water content
492 depresses the silica activity of the melt, which in turn decreases the calculated oxygen fugacity values. We
493 also note that CO_2 has a minor effect on a_{SiO2}^{melt}, however, the magnitude of this effect is insignificant
494 compared to H_2O. Varying CO_2 content from 0 to 2000 ppm changes the a_{SiO2}^{melt} value by 0.003.

This is the peer-reviewed, final accepted version for American Mineralogist, published by the Mineralogical Society of America.
The published version is subject to change. Cite as Authors (Year) Title. American Mineralogist, in press.
DOI: https://doi.org/10.2138/am-2023-9021. http://www.minsocam.org/

Uncertainties in the composition of the equilibrium liquid coexisting with olivine and spinel may impact the calculated a_{SiO2}^{melt} value, however, we stress that uncertainties in the a_{SiO2}^{melt} obtained for tholeiites and olivine tholeiites (a_{SiO2}^{melt} ranging from 0.45 to 0.65) exert minimal leverage on the fO_2 values returned by the model. To illustrate this point, we have performed a sensitivity analysis that shows uncertainties in the a_{SiO2}^{melt} of ± 0.05 (a reasonable assumption for the effects uncertainties in the input liquid composition) generate a response in the returned fO_2 value of approximately ±0.10 log units (Fig. 9), which is significantly smaller than the error estimate of either model. This analysis highlights an important feature intrinsic to the OSaS approach - namely that a reasonable approximation of the input liquid composition may be sufficient for applying the models to fO_2 calculations of basaltic lavas. In other words, small errors in the input liquid composition are not translated into significant errors in the calculated fO_2 values for tholeiites and olivine tholeiites. For liquids with high a_{SiO2}^{melt} values, silica activity is effectively a variable of second order importance. On the other hand, for liquid compositions that have low a_{SiO2}^{melt} values that characterize basanites and feldspathoidal basalts, it is clear that a_{SiO2}^{melt} exerts significant leverage on the resultant fO_2 values (Fig. 10). Therefore, caution should be exercised in applying the OSaS to silica-undersaturated magmas with poorly constrained melt compositions. Though the OSaS models were successfully applied experiments performed on basanites and alkali-rich compositions, we suggest that the models are best applied to magmas with $a_{SiO2}^{melt} > 0.35$ to minimize errors related to intrinsic uncertainties associated with the silica activity values.

We explored the impact of uncertainties in pressure, temperature, and dissolved water content on the fO_2 values calculated from the OSaS formulations by preforming a sensitivity test using the olivine-spinel-glass assemblage from an experiment reported in Grove et al. (2003) (their experiment 85-41c#7). The olivine-spinel and liquid compositions were supplied to the oxybarometers and the assumed values for temperature, pressure, and water content were systematically varied. We find that, for the classical-OSaS oxygen barometer, if temperature is known within ±25°C (at a constant pressure of 200 MPa), the uncertainty in fO_2 is approximately ± 0.3log units (Fig. 11). Increasing the water content of the melt at constant pressure (200 MPa) and temperature, from 1.0 wt. % to 5.0 wt%, generates a decrease in the calculated fO_2 of ~0.40 log units (Fig. 11A). At a constant temperature of 1050°C and dissolved H_2O content of 4 wt. %, the effect of increasing pressure from 100 to 500 MPa generates an increase in the model calculated fO_2 value of less than 0.3 log units. We find similar uncertainties with respect to the effects of temperature, dissolved H_2O content, and pressure when repeating the same test for the MELTS-OSaS oxybarometer (Fig. 11C&D). Provided that one can estimate the crystallization temperature of olivine-spinel pairs to a precision of ±25°C and the dissolved water content of the melt to ±1.5 wt%, both OSaS models should return accurate fO_2 values.

6. Application of the OSaS to Natural Samples

While the OSaS barometers yield accurate fO_2 values for the experimental validation datasets, we have also applied the models to a suite of natural samples, where considerably less is known about the temperature-pressure-H_2O conditions at the time of crystal growth. This application effectively serves as a "field" test that is intended to help establish whether the models generate reasonable estimates of fO_2 for natural samples. We have attempted to apply the OSaS models to olivine-spinel-melt pairs from natural samples that have established values of fO_2, preferably through a method of determining fO_2 other than a strictly thermodynamic approach (i.e., an evaluation of $Fe^{3+}/\sum Fe$ from XANES or Mossbauer Spectroscopy). Though many spectroscopic works on $Fe^{3+}/\sum Fe$ in glasses in melt inclusions often supply the composition of the host olivine, we cannot identify a study that also reports spinel compositions. Therefore, we target olivine- and spinel-bearing mafic rocks that have an existing fO_2 estimates derived from $Fe^{3+}/\sum Fe$ from XANES or Mossbauer Spectroscopy, which are from locations that also have a variety of samples with detailed petrologic descriptions and analyses of olivine, spinel, and glass.

It has long been recognized that the oxidations states recorded by basalt glasses from the midocean ridge (MORBs) provide a record of the oxidation state of their mantle source (Arculus, 1979; Christie et al., 1986; Haggerty, 1978). As such, there has been significant effort exerted in determining the $Fe^{3+}/\sum Fe$ of MOR glasses (Bézos & Humler, 2005; Christie et al., 1986; Cottrell & Kelley, 2011; O'Neill et al., 2018; Zhang et al., 2018), which can be converted to an oxygen fugacity using models from the literature (Jayasuriya et al., 2004; Kress & Carmichael, 1991; O'Neill et al., 2018). In general, the $Fe^{3+}/\sum Fe$ measured for MORBs indicate that these basalts record an oxygen fugacity within approximately ±0.20 log units of the fayalite-magnetite-quartz buffer (e.g., ΔFMQ+0.10±0.18, Cottrell & Kelley, 2011; ΔFMQ–0.17±0.15, Zhang et al. 2018; ΔFMQ+0.19±0.35, O'Neill et al., 2018) (Fig. 12). We examined literature associated with the Deep-Sea Drilling Project (DSPS) and identified studies that report compositions of olivine, spinel and matrix glasses from any midocean ridge. We found olivine, spinel and matrix glasses from the Costa Rican Ridge Zone (leg 70 sample 504B, Group J) (Natland et al., 1983) and from the Lau Basin (Hawkins & Melchior, 1985), which is a complex back arc basin situated between a subduction zone on its eastern side and back arc ridges on its western margin (Baker et al., 2019) (Supplemental Data Table S4). We note that within these studies, some metadata are reported for mineral analyses, such as location on the grain (i.e., core or rim) or if spinels were included in olivine, but reporting of these observations is not consistent from study to study. For the Lau Basin samples, Hawkins and Melchior (1985) and Kamenetsky et al. (1997) report temperatures for the rocks from their study using olivine-melt equilibrium and olivine-chromite equilibrium, and we adopt those temperatures [average from Hawkins and Melchior (1985) = 1190°C] for our application here, along with pressures of 0.1 MPa and H_2O contents of 0 wt.%. We find

that the classical and MELTS-OSaS barometers yield logfO_2 values of -8.33 (±0.1) and -8.42 (±0.07), which correspond to values of ΔQFM+0.09 and -0.02, respectively, for the Lau Basin Basalts. For the Costa Rican Ridge samples, Natland et al. (1983) report several olivine and spinel compositions for a given rock composition. We show the average oxygen fugacity (±1σ) for each sample based on all possible pairings of olivine and spinel for a given liquid composition, where we assume a temperature of 1200°C, a pressure of 0.1 MPa, and H_2O content of 0 wt. % in our calculations (Supplemental Data Table S2). We find that the classical-OSaS and MELTS-OSaS barometers yield logfO_2 values of -8.41 (±0.24) and -8.47 (±0.23), which correspond to ΔFMQ-0.11 and -0.16, respectively, for the Costa Rican Ridge Basalts (Fig. 12). Overall, the oxygen fugacity values generated from the OSaS for these samples agree with the established redox range for MORBs from derived from other methods.

It is also widely accepted that volcanic rocks erupting from subduction zone settings are systematically more oxidized than midocean ridges (Carmichael, 1991; Cottrell et al., 2020), thus we aim to identify arc segments for which there is an estimate of magmatic oxygen fugacity using some spectroscopic method. Brounce et al. (2014) reports oxygen fugacity values derived from Fe K-edge XANES analyses for primitive volcanic glasses from Mariana trough and arc (Fig. 12). Brounce et al. (2014) found that elevated $Fe^{3+}/\sum Fe$ ratios and low MgO contents of whole rock and glass compositions from the Mariana samples suggested that olivine fractionation had occurred prior to eruption. Therefore, Brounce et al. (2014) corrected the measured $Fe^{3+}/\sum Fe$ to reflect the fractionation of olivine from the liquid using the model of Lee et al. (2009). We show ΔFMQ values that correspond to the initial $Fe^{3+}/\sum Fe$ determined by spectroscopy and the ΔFMQ values that correspond to $Fe^{3+}/\sum Fe$ corrected for olivine fractionation. We applied the OSaS models to olivine-spinel-glass data from samples from the Mariana trough and arc from the literature (Bloomer & Hawkins, 1987; Hawkins & Melchior, 1985). Five samples from the Marianas trough have reported temperatures that range from 1084-1197°C, water contents of ~2 wt% to which we ascribe pressures of 100 MPa. We find that the classical-OSaS and MELTS-OSaS oxybarometers yield redox estimates from ΔFMQ +0.3 to +1.3 and +0.1 to +1.5, respectively, for the samples from the Mariana Trough. One sample from the Mariana Arc (Bloomer & Hawkins, 1987) has a reported temperature of 1200°C and H_2O contents of ~2 wt%H_2O, which we adopt for our tests (Supplemental Data Table S4). We assign pressure of olivine crystallization based on the H_2O contents reported for these samples (100 MPa). The classical and MELTS-OSaS oxybarometers yield redox estimates from ΔFMQ +1.9 and +1.5, respectively, for the sample from the Mariana arc. The OSaS-determined redox conditions for the Mariana trough samples span a range that partially overlaps with the oxygen fugacities determined by Brounce et al. (2014), after olivine addition. The redox conditions for samples from the Mariana arc determined by OSaS barometer overlap well with those determined by Brounce et al. (2014).

This is the peer-reviewed, final accepted version for American Mineralogist, published by the Mineralogical Society of America.
The published version is subject to change. Cite as Authors (Year) Title. American Mineralogist, in press.
DOI: https://doi.org/10.2138/am-2023-9021. http://www.minsocam.org/

596 OSaS-model fO_2 estimates for basalts from the Mariana trough exceed the values determined by
597 Brounce et al. (2014). We suspect this difference arises due to treatments of the different dataset; we do not
598 correct the samples in our application for any olivine fractionation. The addition of olivine back into the
599 Mariana trough samples to reconstruct primary liquid compositions will cause the oxygen fugacities in Fig.
600 11 to decrease, towards those of Brounce et al. (2014). We find that the samples from the Mariana trough
601 that yield the highest estimated values of fO_2 also have the lowest MgO contents, suggesting that the olivine-
602 spinel pairs could record evolving fO_2 due to fractionation or melt-vapor separation. We emphasize that
603 numerous redox processes (e.g., degassing, crystallization) occur in magmatic plumbing systems and that
604 the compositions of olivine-spinel pairs may provide a valuable record of these processes. The similarities
605 between the fO_2 estimates from both the Classical and MELTS implementations of the barometers and those
606 from spectroscopic studies lend considerable confidence to fO_2 estimates produced by both
607 implementations of the OSaS models. A caveat to both comparisons is that neither application involves
608 precisely the same sample, however, we note that the fO_2 values returned for each tectonic setting are
609 consistent with the accepted values or those reported in the literature.
610
611 **7. Implications**
612 One potential application of these models is to evaluate the attainment of redox equilibrium that
613 employ solid state buffer assemblages (e.g., the double capsule technique in piston cylinder experiments)
614 in phase equilibrium and crystallization experiments performed on basaltic compositions. The new models
615 offer an accessible method (i.e., one that only requires access to an electron microprobe) for experimental
616 petrologists to ascertain if redox equilibrium was indeed achieved and maintained throughout the duration
617 of an experiment.
618 More importantly, we envision that the OSaS models can potentially facilitate an expansion of
619 magmatic redox studies to samples not amenable to XANES or Mossbauer measurements. Existing
620 magmatic redox studies have been limited to a small number of samples from settings that produce copious
621 quantities of glassy material, however tectonic settings (such as continental rifts) simply do not generate
622 many glassy samples, and thus remain chronically understudied. Furthermore, the OSaS models provide an
623 accessible alternative for researchers who need to generate magmatic redox data but lack access to
624 synchrotron or Mossbauer facilities. We also stress that the OSaS models can serve a key role in cross
625 checking fO_2 values from olivine hosted melt inclusions or rapidly quenched samples derived from
626 spectroscopic measurements against those with recorded cotectic olivine spinel pairs.
627 The application of the OSaS models to natural samples requires that potential users (1) identify
628 equilibrium olivine-spinel pairs in the samples of interest, (2) estimate the cotectic temperature for the
629 olivine-spinel pair, (3) obtain an estimate of the liquid in equilibrium with the olivine-spinel pairs, along

with the H_2O content, and (4) have some constraint on equilibration pressure. Below we offer a few criteria and suggested methods to aid potential users in completing the aforementioned tasks. We recognize that this list of suggestions is not exhaustive and there are other potential methods approaches to assess equilibrium among the phases of interest, to obtain estimates for liquidus temperatures, and to estimate the water content of the melt. Potential OSaS users are under no obligation to employ our suggestions and are encouraged to adapt the tool to their purposes as they see fit, however, we stress that it is incumbent on potential users to exercise sound petrologic judgement when applying the OSaS models.

The identification of disequilibrium olivine-spinel pairs can be accomplished by comparing the $K_{d\ Fe^{2+}\text{-}Mg}^{ol\text{-}sp}$ for the pair of interest with the values predicted by Eq. 12 and/or through the equilibrium evaluation of Li et al. (1995). Though this simple approach does not ensure that a given pair represents an equilibrium assemblage, it does serve as a rough filter to eliminate olivine-spinel pairs that are clearly out of equilibrium and will generate inaccurate fO_2 values. We stress that olivine and Cr-spinel are often the first two liquidus phases in basalts that contain > 6.0 wt. % MgO. In such magmas, spinel is often present in the form of euhedral to subhedral inclusions in the cores of olivine phenocrysts (Roedder et al. 2006). These textures represent cotectic pairs that can be readily identified. We suggest that the OSaS models be applied to samples that experienced rapid cooling after eruption (e.g., surficial lava flows) to minimize potential subsolidus re-equilibration between olivine and spinel.

Of these tasks, obtaining accurate estimates for the olivine-spinel cotectic temperature is the least straightforward. There are several geothermometers that can be used to help estimate olivine-spinel cotectic temperatures (e.g., the olivine liquid geothermometers of Putrika, 2005; Herzberg and O'Hara, 2002), however we suggest that the Al in olivine geothermometer (Coogan et al., 2014; Wan et al., 2008) is well suited to estimate the crystallization temperature for an olivine-spinel pair of interest. The Al in olivine geothermometer is ideally suited for this task as it exploits the temperature dependence of the Al partition coefficient between olivine and spinel and can generate information about the cotectic temperature for the pair. We note that this approach does require careful consideration of EMP detection limits and analytical uncertainties for measured Al concentration of olivine. Thermometers based on Mg-Ni partitioning in olivine (e.g., Pu et al., 2017) may also prove useful for the OSaS, as this method can also provide estimates of pre-eruptive H_2O contents, though we note that laser ablation inductively coupled mass-spectrometry (LA-ICPMS) may be required for successful application of this thermometer. We also suggest that if whole rock compositions are known, the "reasonableness" of the olivine-spinel temperature estimates can be cross checked against the MELTS-predicted liquidus temperature for the olivine composition of interest.

To determine the appropriate liquid composition in equilibrium with olivine spinel pairs for samples that lack glassy groundmass, we suggest that whole rock compositions could be used directly, depending if sample crystallinity is low or if it could be demonstrated that an olivine-spinel pair is in

equilibrium with the whole rock composition. Alternatively, the whole rock composition, mineral compositions, and mineral modes in a rock could be used to calculate a predicted interstitial liquid. In evaluating the combination of any liquid-crystal pair, some equilibrium test, such as the $^{Fe\text{-}Mg}K_D$ values between olivine and melt, can be employed to assess the reasonableness of a selected melt composition. We do emphasize that one of the features of the OSaS model is that the uncertainties in the a_{SiO2}^{melt} obtained for tholeiites and olivine tholeiites (a_{SiO2}^{melt} ranging from 0.45 to 0.65), and therefore, the selected liquid composition, exert minimal leverage on the fO_2 values returned by the model (Fig. 10). We provide a guide in Appendix 2 for arriving at estimates of melt compositions in equilibrium with phenocrysts, using whole rock compositions, mineral compositions, and modes for a Snake River Plane basalt.

For hydrous magmas, the implementation of the OSaS models depends on one being able to estimate the water content of the melt. In the absence melt inclusion data, we suggest that users estimate water content with plagioclase-liquid hygrometry (e.g., Putirka, 2008; Waters and Lange, 2015), or through microbeam studies of melt inclusions where possible. Pressure should be considered when applying the OSaS to non-experimental samples. Careful microbeam studies of dissolved volatiles (e.g., CO_2) in olivine-hosted melt inclusions may also provide constraints on the minimum pressure for olivine crystallization. In many cases it is difficult, if not impossible, to estimate the pressure at which olivine-spinel pairs grew from the liquid, however, we stress that pressure has only a minor effect on the OSaS-determined fO_2 values for pressures < 500 MPa. As such, we strongly recommend that the OSaS should primarily to samples in which the olivine-spinel pairs generated by episodes of shallow crustal crystallization.

Finally, in the supplement, we provide all datasets, a python code with instructions to users, both the classical-OSaS and MELTS-OSaS models that can be uploaded to and used on the Thermoengine website, a benchmark input file that can be modified with a user's data and uploaded along with the python script, as well as benchmark summary output files for the different models. We encourage readers to utilize the instructions to users, as the code is designed to output all variables described in this work.

Acknowledgements

John Naliboff is thanked for assistance with developing the initial coding approach to this project. Yishen Zhang is thanked for detailed comments and feedback in review that led to improvements on this manuscript. We also acknowledge Fred Davis for his comments on the manuscript. Chip Lesher, the handling editor for this manuscript, is additionally thanked for his feedback and comments on the manuscript.

Figure Captions:

698

699 Figure 1: (A) The olivine-liquid $^{Fe\text{-}Mg}K_D$ values for olivine melt pairs from experiments are shown as a
700 function of the total alkali content of the liquid, where the $^{Fe\text{-}Mg}K_D$ values are calculated using the Fe^{2+}
701 contents in the glasses determined based on the reported temperature, pressures, oxygen fugacities, glass
702 compositions and the empirically calibrated equation of Kress & Carmichael (1991). The $^{Fe\text{-}Mg}K_D$ value of
703 0.3 is shown as a solid black line and grey dashed lines correspond to the $^{Fe\text{-}Mg}K_D$ of 0.3±0.08. Anomalously
704 high and low K_D values and those from experiments that failed additional tests (light colored symbols that
705 fall above or below the dashed grey lines) were flagged as potentially representing poor analyses or
706 disequilibrium. (B) The olivine-spinel $^{Fe\text{-}Mg}K_D$ values calculated for the experimental dataset are shown as
707 a function of the Al content of the spinel. Values that plot significantly (>±0.1) off the linear trend were
708 discarded from the calibration. (C) A plot of the $\log a^{melt}_{SiO2}$ calculated using Eq. 2 rearranged to solve for
709 a^{melt}_{SiO2} using the $\Delta_r G°$, $a^{sp}_{Fe_3O_4}$, the $a^{oliv}_{Fe_2SiO_4}$ and the reported values of fO_2. Experiments that plot in the quartz
710 stability field or plot in the feldspathoid stability field and lack those minerals in their reported run products
711 were excluded from the calibration data set.

712

713 Figure 2: Experiments that passed all exclusionary criteria (e.g., Fig. 1) are shown as a function of their
714 SiO_2 contents and total alkali contents to illustrate the compositional of the dataset. (Auwera & Longhi,
715 1994; Barclay & Carmichael, 2004; Davis & Cottrell, 2018; Feig et al., 2010; Grove et al., 1997, 2003;
716 Grove & Bryan, 1983; Grove & Juster, 1989; Kawamoto, 1996; Krawczynski et al., 2012; Médard & Grove,
717 2008; Meen, 1987, 1990; Pichavant & Macdonald, 2007; Sack et al., 1987; Waters et al., 2021)

718

719 Figure 3: The reported fO_2 values (i.e., log fO_2 known) for the experimental dataset are shown with their
720 calculated values of fO_2 using the classical OSaS oxygen barometer. The symbols are color coded to
721 represent the Cr content of the spinel composition used in the calculation. The classical OSaS model (using
722 MELTS generated silica activity values referenced to tridymite and activity models from the literature)
723 reproduces the experimental fO_2 values with an average RMSE of ±0.40 log units and an average residual
724 of ±0.32. The fO_2 values generated by the classical OSaS model do not covary with spinel composition.

725

726 Figure 4: In all panels, the residuals (known fO_2-modeled fO_2) from the classical OSaS barometer are
727 shown as a function of various input parameters: (A) wt. % SiO_2, where symbols are color coded to total
728 alkali content, (B) experimental temperature, where symbols are color coded to experimental pressure
729 (MPa), (C) dissolved water content of the melt, where symbols are color coded to experimental pressure
730 (MPa), (D) Mg content of the experimental olivine, where symbols are color coded to the Cr#
731 ($X_{Cr}/(X_{Cr}+X_{Al})$ in spinel.

Figure 5: The reported fO_2 values (i.e., log fO_2 known) for the validation dataset are plotted against the fO_2 using the predicted MELTS-OSaS; this plot illustrates how the uncorrected version of MELTs-OSaS reproduces reported fO_2 values for experiments that have spinel with low Cr concentrations and underpredicts fO_2 values for experiments that have spinel with Cr content.

Figure 6: (A) The residuals from the MELTS OSaS are plotted against Cr# of the spinel; this plot shows a strong correlation between the Cr content of the spinel and the observed fO_2 residual. (B) The residuals of the MELTS OSaS plotted against the mol. % fayalite in the olivine.

Figure 7: (A) The MELTS μFe_3O_4 values (black diamonds) and the corrected μFe_3O_4 values (grey circles) are shown, as a function of the equilibrium μFe_3O_4 values (i.e., the values of μFe_3O_4 required to successfully predict the experimental fO_2 values). The μFe_3O_4 values directly output from MELTs fall below the 1:1 line, indicating that they will under predict values of fO_2. The corrected μFe_3O_4 values match well with the 1:1 line suggesting that they accurately reproduce the reported values of values of fO_2. (B) The reported fO_2 values (i.e., log fO_2 known) for the experimental validation dataset are shown with their calculated values of fO_2 using the calibrated MELTS OSaS with the corrected μFe_3O_4 values. (C) The reported fO_2 values (i.e., log fO_2 known) for 18 experiments from the studies of Krawczynski et al (2012), Gaetani et al. (1994), Takagi et al. (2005), Melekova et al. (2017), and Zhang et al. (2023) that were not a part of the initial validation/calibration dataset used to generate the μFe_2O_3 correction are plotted against the fO_2 values predicted from the calibrated MELTS-OSaS model. MELTS-OSaS reproduces the 18 experimental fO_2 values with an average RMSE of ±0.23 log units, a standard error estimate of ±0.20, and an average residual of ±0.18.

Figure 8: In all panels, the residuals (known fO_2-modeled fO_2) from the MELTS OSaS model (with μFe_3O_4 correction) are shown as a function of various input parameters: (A) wt.% SiO_2, where symbols are color coded to total alkali content, (B) experimental temperature, where symbols are color coded to experimental pressure (MPa), (C) dissolved water content of the melt, where symbols are color coded to experimental pressure (MPa), (D) Mg content of the experimental olivine, where symbols are color coded to the Cr# ($X_{Cr}/(X_{Cr}+X_{Al})$ in spinel.

Figure 9: The fO_2 values calculated for the experimental dataset from the classical OSaS model plotted against the values calculated from the MELTS-OSaS (with μFe_3O_4 correction). The plot shows a 1:1 line as well as the equation derived from a linear regression of the plotted data.

Figure 10: The curve in this figure shows how the OSaS predicted fO_2 values vary as a function of a_{SiO2}^{melt} for a fictive olivine-spinel pair with fixed composition activity values and a fixed temperature of 1150°C. The symbols with the error bars on the curve illustrate the magnitude of the error in the predicted fO_2 value assuming a that MELTS generated a_{SiO2}^{melt} values have an intrinsic uncertainty of ±0.05. The a_{SiO2}^{melt} and fO_2 values for the experimental validation dataset are superimposed on this plot to illustrate that most "basaltic" magma compositions (even alkali-rich basalts) characterized by a_{SiO2}^{melt} values that correspond to low uncertainties in OSaS derived fO_2 values.

Figure 11: (A) The effect of variable water content impacts the melts derived silica activity and the calculated fO_2 values across a range of temperatures (at constant pressure of 200 MPa) for the classical-OSaS model. (B) The effect of pressure variation on calculated fO_2 values as a function of temperature ($\Delta_r G$ values are calculated for each curve at the temperatures at which they appear on the plot) is shown for the classical-OSaS model. (C) The effect of variable water content on the MELTS-derived silica activity and the calculated fO_2 values is shown for a range of temperatures (at constant pressure) using the MELTS-OSaS model. (D) The effect of pressure variation on the calculated values of fO_2 is shown for the MELTS-OSaS model.

Figure 12 : The fO_2 values (relative to the FMQ buffer) calculated from the OSaS models for the MORB samples from the Lau Basin (1, Hawkins & Melchior, 1985; 2, Kamenetsky et al., 1997), Costa Rican Ridge Zone (3, Natland et al., 1983), and basalts from the Mariana Trough (1, Hawkins & Melchior, 1985) and Arc (7, Bloomer & Hawkins, 1987) are shown with the fO_2 values determined by XANES for midocean ridge basalt glasses (4, Zhang et al., 2018; 5, O'Neill et al., 2018) and basalt glasses from the Mariana Trough and Arc basalts (6, Brounce et al., 2014). Brounce et al. (2014) report the $Fe^{3+}/\sum Fe$ ratios for glasses from the Mariana trough in their supplement; we convert these ratios to ΔFMQ values using a temperature of 1150°C the model of Kress and Carmichael (1991). The OSaS-generated values broadly agree with the XANES-established oxygen fugacity values, where there is less agreement in the Mariana trough samples, but excellent agreement between analyses from MORB and general agreement with samples from the Mariana arc (see text).

10. References

Arculus, R. J. (1979). Silica activity and the classification of alkalic and tholeiitic basalts. *American Mineralogist*, *64*(3–4), 436–439.

Auwera, J. V., & Longhi, J. (1994). Experimental study of a jotunite (hypersthene monzodiorite): Constraints on the parent magma composition and crystallization conditions (P, T, f O 2) of the Bjerkreim-Sokndal layered intrusion (Norway). *Contributions to Mineralogy and Petrology*, *118*(1), 60–78. https://doi.org/10.1007/BF00310611

Bai, Q., Mackwell, S. J., & Kohlstedt, D. L. (1991). High-temperature creep of olivine single crystals 1. Mechanical results for buffered samples. *Journal of Geophysical Research: Solid Earth*, *96*(B2), 2441–2463. https://doi.org/10.1029/90JB01723

Baker, E. T., Walker, S. L., Massoth, G. J., & Resing, J. A. (2019). The NE Lau Basin: Widespread and Abundant Hydrothermal Venting in the Back-Arc Region Behind a Superfast Subduction Zone. *Frontiers in Marine Science*, *6*. https://www.frontiersin.org/articles/10.3389/fmars.2019.00382

Ballhaus, C., Berry, R. F., & Green, D. H. (1991). High pressure experimental calibration of the olivine-orthopyroxene-spinel oxygen geobarometer: Implications for the oxidation state of the upper mantle. *Contributions to Mineralogy and Petrology*, *107*(1), 27–40. https://doi.org/10.1007/BF00311183

Barclay, J., & Carmichael, I. S. E. (2004). A Hornblende Basalt from Western Mexico: Water-saturated Phase Relations Constrain a Pressure–Temperature Window of Eruptibility. *Journal of Petrology*, *45*(3), 485–506. https://doi.org/10.1093/petrology/egg091

Berman, R. G. (1988). Internally-Consistent Thermodynamic Data for Minerals in the System Na2O-K2O-CaO-MgO-FeO-Fe2O3-Al2O3-SiO2-TiO2-H2O-CO2. *Journal of Petrology*, *29*(2), 445–522. https://doi.org/10.1093/petrology/29.2.445

Berry, A. J., Shelley, J. M. G., Foran, G. J., O'Neill, H. S. C., & Scott, D. R. (2003). A furnace design for XANES spectroscopy of silicate melts under controlled oxygen fugacities and temperatures to 1773 K. *Journal of Synchrotron Radiation*, *10*(4), Article 4. https://doi.org/10.1107/S0909049503007556

Bézos, A., & Humler, E. (2005). The Fe3+/ΣFe ratios of MORB glasses and their implications for mantle melting. *Geochimica et Cosmochimica Acta*, *69*(3), 711–725. https://doi.org/10.1016/j.gca.2004.07.026

Birner, S. K., Cottrell, E., Warren, J. M., Kelley, K. A., & Davis, F. A. (2018). Peridotites and basalts reveal broad congruence between two independent records of mantle fO2 despite local redox heterogeneity. *Earth and Planetary Science Letters*, *494*, 172–189. https://doi.org/10.1016/j.epsl.2018.04.035

Bloomer, S. H., & Hawkins, J. W. (1987). Petrology and geochemistry of boninite series volcanic rocks from the Mariana trench. *Contributions to Mineralogy and Petrology*, *97*(3), 361–377. https://doi.org/10.1007/BF00371999

Brounce, M. N., Kelley, K. A., & Cottrell, E. (2014). Variations in Fe3+/∑Fe of Mariana Arc Basalts and Mantle Wedge fO2. *Journal of Petrology*, *55*(12), 2513–2536. https://doi.org/10.1093/petrology/egu065

Bucholz, C. E., & Kelemen, P. B. (2019). Oxygen fugacity at the base of the Talkeetna arc, Alaska. *Contributions to Mineralogy and Petrology*, *174*(10), 79. https://doi.org/10.1007/s00410-019-1609-z

Buddington, A. F., & Lindsley, D. H. (1964). Iron-Titanium Oxide Minerals and Synthetic Equivalents. *Journal of Petrology*, *5*(2), 310–357. https://doi.org/10.1093/petrology/5.2.310

Carmichael, I. S. E. (1991). The redox states of basic and silicic magmas: A reflection of their source regions? *Contributions to Mineralogy and Petrology*, *106*(2), 129–141. https://doi.org/10.1007/BF00306429

Carmichael, I. S. E., Nicholls, J., & Smith, A. L. (1970). Silica activity in igneous rocks. *American Mineralogist*, *55*(1–2), 246–263.

Christie, D. M., Carmichael, I. S. E., & Langmuir, C. H. (1986). Oxidation states of mid-ocean ridge basalt glasses. *Earth and Planetary Science Letters*, *79*(3), 397–411. https://doi.org/10.1016/0012-821X(86)90195-0

Cline Ii, C. J., Faul, U. H., David, E. C., Berry, A. J., & Jackson, I. (2018). Redox-influenced seismic properties of upper-mantle olivine. *Nature*, *555*(7696), 355–358. https://doi.org/10.1038/nature25764

Coogan, L. A., Saunders, A. D., & Wilson, R. N. (2014). Aluminum-in-olivine thermometry of primitive basalts: Evidence of an anomalously hot mantle source for large igneous provinces. *Chemical Geology*, *368*, 1–10. https://doi.org/10.1016/j.chemgeo.2014.01.004

Cottrell, E., Birner, S., Brounce, M., Davis, F., Waters, L., & Kelley, K. (2020). *OXYGEN FUGACITY ACROSS TECTONIC SETTINGS* [Preprint]. Geology. https://doi.org/10.1002/essoar.10502445.1

Cottrell, E., & Kelley, K. A. (2011). The oxidation state of Fe in MORB glasses and the oxygen fugacity of the upper mantle. *Earth and Planetary Science Letters*, *305*(3–4), 270–282. https://doi.org/10.1016/j.epsl.2011.03.014

Dachs, E., & Geiger, C. A. (2007). Letter: Entropies of mixing and subsolidus phase relations of forsterite□fayalite (Mg2SiO4□Fe2SiO4) solid solution. *American Mineralogist*, *92*(4), 699–702. https://doi.org/10.2138/am.2007.2465

Davis, F. A., & Cottrell, E. (2018). Experimental investigation of basalt and peridotite oxybarometers: Implications for spinel thermodynamic models and Fe3+ compatibility during generation of upper mantle melts. *American Mineralogist*, *103*(7), 1056–1067. https://doi.org/10.2138/am-2018-6280

Davis, F. A., & Cottrell, E. (2021). Partitioning of Fe2O3 in peridotite partial melting experiments over a range of oxygen fugacities elucidates ferric iron systematics in mid-ocean ridge basalts and ferric iron content of the upper mantle. *Contributions to Mineralogy and Petrology*, *176*(9), 67. https://doi.org/10.1007/s00410-021-01823-3

Deng, J., Du, Z., Karki, B. B., Ghosh, D. B., & Lee, K. K. M. (2020). A magma ocean origin to divergent redox evolutions of rocky planetary bodies and early atmospheres. *Nature Communications*, *11*(1), 2007. https://doi.org/10.1038/s41467-020-15757-0

Feig, S. T., Koepke, J., & Snow, J. E. (2010). Effect of oxygen fugacity and water on phase equilibria of a hydrous tholeiitic basalt. *Contributions to Mineralogy and Petrology*, *160*(4), 551–568. https://doi.org/10.1007/s00410-010-0493-3

Frost, D. J., & McCammon, C. A. (2008). The Redox State of Earth's Mantle. *Annual Review of Earth and Planetary Sciences*, *36*(1), 389–420. https://doi.org/10.1146/annurev.earth.36.031207.124322

Gaetani, G.A., Grove, T.L, Bryan, W.B. (1994) 32. Experimental phase relations of basaltic andesite from hole 839B under hydrous and anhydrous conditions. In: Proceeding of the Ocean Drilling Program, Scientific Results, Vol. 135. Eds. Hawkins, J, Parson, L., Allan, J. et al.

887 Gaillard, F., & Scaillet, B. (2014). A theoretical framework for volcanic degassing chemistry in a
888 comparative planetology perspective and implications for planetary atmospheres. *Earth*
889 *and Planetary Science Letters*, *403*, 307–316. https://doi.org/10.1016/j.epsl.2014.07.009
890 Ghiorso, M. S., & Evans, B. W. (2008). Thermodynamics of Rhombohedral Oxide Solid
891 Solutions and a Revision of the FE-TI Two-Oxide Geothermometer and Oxygen-
892 Barometer. *American Journal of Science*, *308*(9), 957–1039.
893 https://doi.org/10.2475/09.2008.01
894 Ghiorso, M. S., & Gualda, G. A. R. (2015). An H2O–CO2 mixed fluid saturation model
895 compatible with rhyolite-MELTS. *Contributions to Mineralogy and Petrology*, *169*(6),
896 53. https://doi.org/10.1007/s00410-015-1141-8
897 Ghiorso, M. S., & Sack, R. O. (1995). Chemical mass transfer in magmatic processes IV. A
898 revised and internally consistent thermodynamic model for the interpolation and
899 extrapolation of liquid-solid equilibria in magmatic systems at elevated temperatures and
900 pressures. *Contributions to Mineralogy and Petrology*, *119*(2), 197–212.
901 https://doi.org/10.1007/BF00307281
902 Grove, T. L., & Bryan, W. B. (1983). Fractionation of pyroxene-phyric MORB at low pressure:
903 An experimental study. *Contributions to Mineralogy and Petrology*, *84*(4), 293–309.
904 https://doi.org/10.1007/BF01160283
905 Grove, T. L., Donnelly-Nolan, J. M., & Housh, T. (1997). Magmatic processes that generated the
906 rhyolite of Glass Mountain, Medicine Lake volcano, N. California. *Contributions to*
907 *Mineralogy and Petrology*, *127*(3), 205–223. https://doi.org/10.1007/s004100050276
908 Grove, T. L., Elkins-Tanton, L. T., Parman, S. W., Chatterjee, N., Muntener, O., & Gaetani, G.
909 A. (2003). Fractional crystallization and mantle-melting controls on calc-alkaline
910 differentiation trends. *Contributions to Mineralogy and Petrology*, *145*(5), 515–533.
911 https://doi.org/10.1007/s00410-003-0448-z
912 Grove, T. L., & Juster, T. C. (1989). Experimental investigations of low-Ca pyroxene stability
913 and olivine-pyroxene-liquid equilibria at 1-atm in natural basaltic and andesitic liquids.
914 *Contributions to Mineralogy and Petrology*, *103*(3), 287–305.
915 https://doi.org/10.1007/BF00402916
916 Gualda, G. A. R., Ghiorso, M. S., Lemons, R. V., & Carley, T. L. (2012). Rhyolite-MELTS: A
917 Modified Calibration of MELTS Optimized for Silica-rich, Fluid-bearing Magmatic
918 Systems. *Journal of Petrology*, *53*(5), 875–890. https://doi.org/10.1093/petrology/egr080
919 Haggerty, S. E. (1978). The redox state of planetary basalts. *Geophysical Research Letters*, *5*(6),
920 443–446. https://doi.org/10.1029/GL005i006p00443
921 Hawkins, J. W., & Melchior, J. T. (1985). Petrology of Mariana Trough and Lau Basin basalts.
922 *Journal of Geophysical Research: Solid Earth*, *90*(B13), 11431–11468.
923 https://doi.org/10.1029/JB090iB13p11431
924 Herzberg, C., & O'Hara, M. J. (2002). Plume-Associated Ultramafic Magmas of Phanerozoic
925 Age. *Journal of Petrology*, *43*(10), 1857–1883.
926 https://doi.org/10.1093/petrology/43.10.1857
927 Hirschmann, M. M. (2012). Magma ocean influence on early atmosphere mass and composition.
928 *Earth and Planetary Science Letters*, *341–344*, 48–57.
929 https://doi.org/10.1016/j.epsl.2012.06.015
930 Hirschmann, M. M., Ghiorso, M. S., Davis, F. A., Gordon, S. M., Mukherjee, S., Grove, T. L.,
931 Krawczynski, M., Medard, E., & Till, C. B. (2008). Library of Experimental Phase
932 Relations (LEPR): A database and Web portal for experimental magmatic phase

equilibria data. *Geochemistry, Geophysics, Geosystems*, *9*(3). https://doi.org/10.1029/2007GC001894

Hou, T., Botcharnikov, R., Moulas, E., Just, T., Berndt, J., Koepke, J., Zhang, Z., Wang, M., Yang, Z., & Holtz, F. (2020). Kinetics of Fe–Ti Oxide Re-equilibration in Magmatic Systems: Implications for Thermo-oxybarometry. *Journal of Petrology*, *61*(egaa116). https://doi.org/10.1093/petrology/egaa116

Jayasuriya, K. D., O'neill, H. S. C., Berry, A. J., & Campbell, S. J. (2004). A Mössbauer study of the oxidation state of Fe in silicate melts. *American Mineralogist*, *89*(11–12), 1597–1609. https://doi.org/10.2138/am-2004-11-1203

Kamenetsky, V. S., Crawford, A. J., Eggins, S., & Mühe, R. (1997). Phenocryst and melt inclusion chemistry of near-axis seamounts, Valu Fa Ridge, Lau Basin: Insight into mantle wedge melting and the addition of subduction components. *Earth and Planetary Science Letters*, *151*(3), 205–223. https://doi.org/10.1016/S0012-821X(97)81849-3

Kawamoto, T. (1996). Experimental constraints on differentiation and H2O abundance of calc-alkaline magmas. *Earth and Planetary Science Letters*, *144*(3), 577–589. https://doi.org/10.1016/S0012-821X(96)00182-3

Krawczynski, M. J., Grove, T. L., & Behrens, H. (2012). Amphibole stability in primitive arc magmas: Effects of temperature, H2O content, and oxygen fugacity. *Contributions to Mineralogy and Petrology*, *164*(2), 317–339. https://doi.org/10.1007/s00410-012-0740-x

Kress, V. C., & Carmichael, I. S. E. (1991). The compressibility of silicate liquids containing Fe2O3 and the effect of composition, temperature, oxygen fugacity and pressure on their redox states. *Contributions to Mineralogy and Petrology*, *108*(1), 82–92. https://doi.org/10.1007/BF00307328

Kurepin, V. A., (2005) A Thermodynamic Model for Fe-Cr Spinels. *Contributions to Mineralogy and Petrology.* 149, 591-599. DOI10.1007/s00410-005-0669-4

Lee, C.-T. A., Luffi, P., Plank, T., Dalton, H., & Leeman, W. P. (2009). Constraints on the depths and temperatures of basaltic magma generation on Earth and other terrestrial planets using new thermobarometers for mafic magmas. *Earth and Planetary Science Letters*, *279*(1–2), 20–33. https://doi.org/10.1016/j.epsl.2008.12.020

Marxer, F., Ulmer, P., & Müntener, O. (2021). Polybaric fractional crystallisation of arc magmas: An experimental study simulating trans-crustal magmatic systems. *Contributions to Mineralogy and Petrology*, *177*(1), 3. https://doi.org/10.1007/s00410-021-01856-8

Matzen, A. K., Baker, M. B., Beckett, J. R., & Stolper, E. M. (2011). Fe–Mg Partitioning between Olivine and High-magnesian Melts and the Nature of Hawaiian Parental Liquids. *Journal of Petrology*, *52*(7–8), 1243–1263. https://doi.org/10.1093/petrology/egq089

Médard, E., & Grove, T. L. (2008). The effect of H2O on the olivine liquidus of basaltic melts: Experiments and thermodynamic models. *Contributions to Mineralogy and Petrology*, *155*(4), 417–432. https://doi.org/10.1007/s00410-007-0250-4

Meen, J. K. (1987). Formation of shoshonites from calcalkaline basalt magmas: Geochemical and experimental constraints from the type locality. *Contributions to Mineralogy and Petrology*, *97*(3), 333–351. https://doi.org/10.1007/BF00371997

Meen, J. K. (1990). Elevation of potassium content of basaltic magma by fractional crystallization: The effect of pressure. *Contributions to Mineralogy and Petrology*, *104*(3), 309–331. https://doi.org/10.1007/BF00321487

Melekhova, E., Blundy, J., Robertson, R., & Humphreys, M. C. S. (2015). Experimental Evidence for Polybaric Differentiation of Primitive Arc Basalt beneath St. Vincent, Lesser Antilles. *Journal of Petrology*, *56*(1), 161–192. https://doi.org/10.1093/petrology/egu074

Moussallam, Y., Edmonds, M., Scaillet, B., Peters, N., Gennaro, E., Sides, I., & Oppenheimer, C. (2016). The impact of degassing on the oxidation state of basaltic magmas: A case study of Kīlauea volcano. *Earth and Planetary Science Letters*, *450*, 317–325. https://doi.org/10.1016/j.epsl.2016.06.031

Natland, J. H., Adamson, A. C., Laverne, C., Melson, W. G., & O'Hearn, T. (1983). A compositionally nearly steady-state magma chamber at the Costa Rica Rift: Evidence from basalt glass and mineral data, Deep Sea Drilling Project Sites 501, 504, and 505. In J. R. Cann, M. G. Langseth, J. Honnorez, R. P. Von Herzen, S. M. White, & et al. (Eds.), *Initial Reports. Deep Sea Drilling Project* (Vol. 69, pp. 811–858). Washington (U.S. Government Printing Office).

Nell, J., & Wood, B. J. (1991). High-temperature electrical measurements and thermodynamic properties of Fe3O4-FeCr2O4-MgCr2O4-FeAl2O4 spinels. *American Mineralogist*, *76*(3–4), 405–426.

Nikolaev, G. S., Ariskin, A. A., & Barmina, G. S. (2018). SPINMELT-2.0: Simulation of Spinel–Melt Equilibrium in Basaltic Systems under Pressures up to 15 Kbar: II. Description of the Program Package, the Topology of the Cr-spinel–Melt Model System, and Petrological Implications. *Geochemistry International*, *56*(2), 125–135. https://doi.org/10.1134/S0016702918020052

O'Neill, H. St. C., Berry, A. J., & Mallmann, G. (2018). The oxidation state of iron in Mid-Ocean Ridge Basaltic (MORB) glasses: Implications for their petrogenesis and oxygen fugacities. *Earth and Planetary Science Letters*, *504*, 152–162. https://doi.org/10.1016/j.epsl.2018.10.002

O'Neill, H. St. C., Pownceby, M. I., & McCammon, C. A. (2003). The magnesiow□stite: Iron equilibrium and its implications for the activity-composition relations of (Mg,Fe)2SiO4 olivine solid solutions. *Contributions to Mineralogy and Petrology*, *146*(3), 308–325. https://doi.org/10.1007/s00410-003-0496-4

Ortenzi, G., Noack, L., Sohl, F., Guimond, C. M., Grenfell, J. L., Dorn, C., Schmidt, J. M., Vulpius, S., Katyal, N., Kitzmann, D., & Rauer, H. (2020). Mantle redox state drives outgassing chemistry and atmospheric composition of rocky planets. *Scientific Reports*, *10*, 10907. https://doi.org/10.1038/s41598-020-67751-7

Pichavant, M., & Macdonald, R. (2007). Crystallization of primitive basaltic magmas at crustal pressures and genesis of the calc-alkaline igneous suite: Experimental evidence from St Vincent, Lesser Antilles arc. *Contributions to Mineralogy and Petrology*, *154*(5), 535–558. https://doi.org/10.1007/s00410-007-0208-6

Putirka, K. D. (2005). Mantle potential temperatures at Hawaii, Iceland, and the mid-ocean ridge system, as inferred from olivine phenocrysts: Evidence for thermally driven mantle plumes. *Geochemistry, Geophysics, Geosystems*, *6*(5). https://doi.org/10.1029/2005GC000915

Putirka, K. D. (2008). Thermometers and Barometers for Volcanic Systems. *Reviews in Mineralogy and Geochemistry*, *69*(1), 61–120. https://doi.org/10.2138/rmg.2008.69.3

Roeder, P., Gofton, E., & Thornber, C. (2006). Cotectic Proportions of Olivine and Spinel in Olivine-Tholeiitic Basalt and Evaluation of Pre-Eruptive Processes. *Journal of Petrology*, *47*(5), 883–900. https://doi.org/10.1093/petrology/egi099

Sack, R. O., & Ghiorso, M. S. (1989). Importance of considerations of mixing properties in establishing an internally consistent thermodynamic database: Thermochemistry of minerals in the system Mg2SiO4-Fe2SiO4-SiO2. *Contributions to Mineralogy and Petrology*, *102*(1), 41–68. https://doi.org/10.1007/BF01160190

Sack, R. O., & Ghiorso, M. S. (1991a). An internally consistent model for the thermodynamic properties of Fe?Mg-titanomagnetite-aluminate spinels. *Contributions to Mineralogy and Petrology*, *106*(4), 474–505. https://doi.org/10.1007/BF00321989

Sack, R.O. & Ghiorso, M.S. (1991b) Chromian Spinels as Petrogenetic Indicators: Thermodynamics and Petrological Applications. American Mineralogist, 76, 827-847

Sack, R. O., Walker, D., & Carmichael, I. S. E. (1987). Experimental petrology of alkalic lavas: Constraints on cotectics of multiple saturation in natural basic liquids. *Contributions to Mineralogy and Petrology*, *96*(1), 1–23. https://doi.org/10.1007/BF00375521

Sisson, T. W., & Grove, T. L. (1993). Temperatures and H2O contents of low-MgO high-alumina basalts. *Contributions to Mineralogy and Petrology*, *113*(2), 167–184. https://doi.org/10.1007/BF00283226

Sossi, P. A., Burnham, A. D., Badro, J., Lanzirotti, A., Newville, M., & O'Neill, H. S. C. (2020). Redox state of Earth's magma ocean and its Venus-like early atmosphere. *Science Advances*, *6*(48), eabd1387. https://doi.org/10.1126/sciadv.abd1387

Stolper, E. M., Shorttle, O., Antoshechkina, P. M., & Asimow, P. D. (2020). The effects of solid-solid phase equilibria on the oxygen fugacity of the upper mantle. *American Mineralogist*, *105*(10), 1445–1471. https://doi.org/10.2138/am-2020-7162

Takagi, D., Sato, H., & Nakagawa, M. (2005). Experimental study of a low-alkali tholeiite at 1–5 kbar: Optimal condition for the crystallization of high-An plagioclase in hydrous arc tholeiite. *Contributions to Mineralogy and Petrology*, *149*(5), 527–540. https://doi.org/10.1007/s00410-005-0666-7

Thermoengine, C. C. (2022). *Thermoengin: SOftware for Modl Building and Computational Thermodynamics Supporting Application in the Earth Sciences (1.0.0) Zenodo.* https://doi.org/10.5281/zenodo.6527840

Toplis, M. J. (2005). The thermodynamics of iron and magnesium partitioning between olivine and liquid: Criteria for assessing and predicting equilibrium in natural and experimental systems. *Contributions to Mineralogy and Petrology*, *149*(1), 22–39. https://doi.org/10.1007/s00410-004-0629-4

Wan, Z., Coogan, L., & Canil, D. (2008). Experimental calibration of aluminum partitioning between olivine and spinel as a Geothermometer. *American Mineralogist - AMER MINERAL*, *93*, 1142–1147. https://doi.org/10.2138/am.2008.2758

Waters, L. E., Cottrell, E., Coombs, M. L., & Kelley, K. A. (2021). Generation of Calc-Alkaline Magmas during Crystallization at High Oxygen Fugacity: An Experimental and Petrologic Study of Tephras from Buldir Volcano, Western Aleutian Arc, Alaska, USA. *Journal of Petrology*, *62*(3). https://doi.org/10.1093/petrology/egaa104

Waters, L., & Lange, R. (2015). An updated calibration of the plagioclase-liquid hygrometer-thermometer applicable to basalts through rhyolites. *American Mineralogist*, *100*, 2172–2184. https://doi.org/10.2138/am-2015-5232

Wood, B. J. (1990). An experimental test of the spinel peridotite oxygen barometer. *Journal of Geophysical Research: Solid Earth*, *95*(B10), 15845–15851. https://doi.org/10.1029/JB095iB10p15845

Zhang, H. L. (2019). *Advances of ferrous and ferric Mossbauer recoilless fractions in minerals and glasses | Elsevier Enhanced Reader*. https://doi.org/10.1016/j.gsf.2021.101316

Zhang, H. L., Cottrell, E., Solheid, P. A., Kelley, K. A., & Hirschmann, M. M. (2018). Determination of Fe3+/ΣFe of XANES basaltic glass standards by Mössbauer spectroscopy and its application to the oxidation state of iron in MORB. *Chemical Geology*, *479*, 166–175. https://doi.org/10.1016/j.chemgeo.2018.01.006

Zhang, Y., Namur, O., & Charlier, B. (2023). Experimental study of high-Ti and low-Ti basalts: Liquid lines of descent and silicate liquid immiscibility in large igneous provinces. *Contributions to Mineralogy and Petrology*, *178*(1), 7. https://doi.org/10.1007/s00410-022-01990-x

Zhang, Y., Hou, T., Veksler, I. V., Lesher, C. E., & Namur, O. (2018). Phase equilibria and geochemical constraints on the petrogenesis of high-Ti picrite from the Paleogene East Greenland flood basalt province. *Lithos*, *300–301*, 20–32. https://doi.org/10.1016/j.lithos.2017.11.011

Table 1: Linear Regression Parameters for μFe_3O_4 *Correction*				
	Coefficients	*Standard Error*	*t Stat*	*P-value*
Intercept	-88317.12	30632.35	-2.88	6.02E-03
MELTS μFe_3O_4	0.9680702	0.02	56.66	1.73E-43
X_i *Spinel*				
Cr_2O_3	66581.75	11814.68	5.64	1.08E-06
FeO^T	53625.74	12355.58	4.34	7.96E-05
MgO	75747.29	20637.63	3.67	6.40E-04

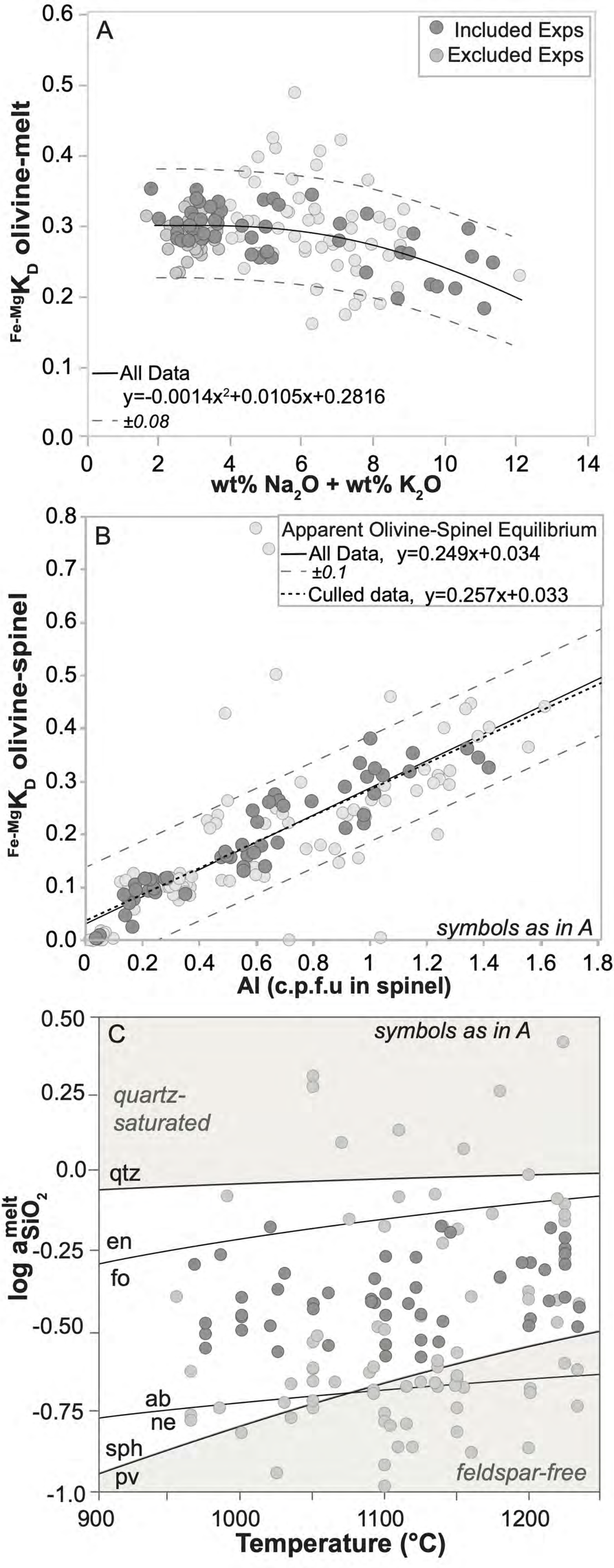
A
Included Exps
Excluded Exps
$^{Fe-Mg}K_D$ olivine-melt
All Data
y=-0.0014x²+0.0105x+0.2816
±0.08
wt% Na_2O + wt% K_2O
B
Apparent Olivine-Spinel Equilibrium
All Data, y=0.249x+0.034
±0.1
Culled data, y=0.257x+0.033
symbols as in A
$^{Fe-Mg}K_D$ olivine-spinel
Al (c.p.f.u in spinel)
C
symbols as in A
quartz-saturated
qtz
en
fo
ab
ne
sph
pv
feldspar-free
$\log a^{melt}_{SiO_2}$
Temperature (°C)

Figure 1

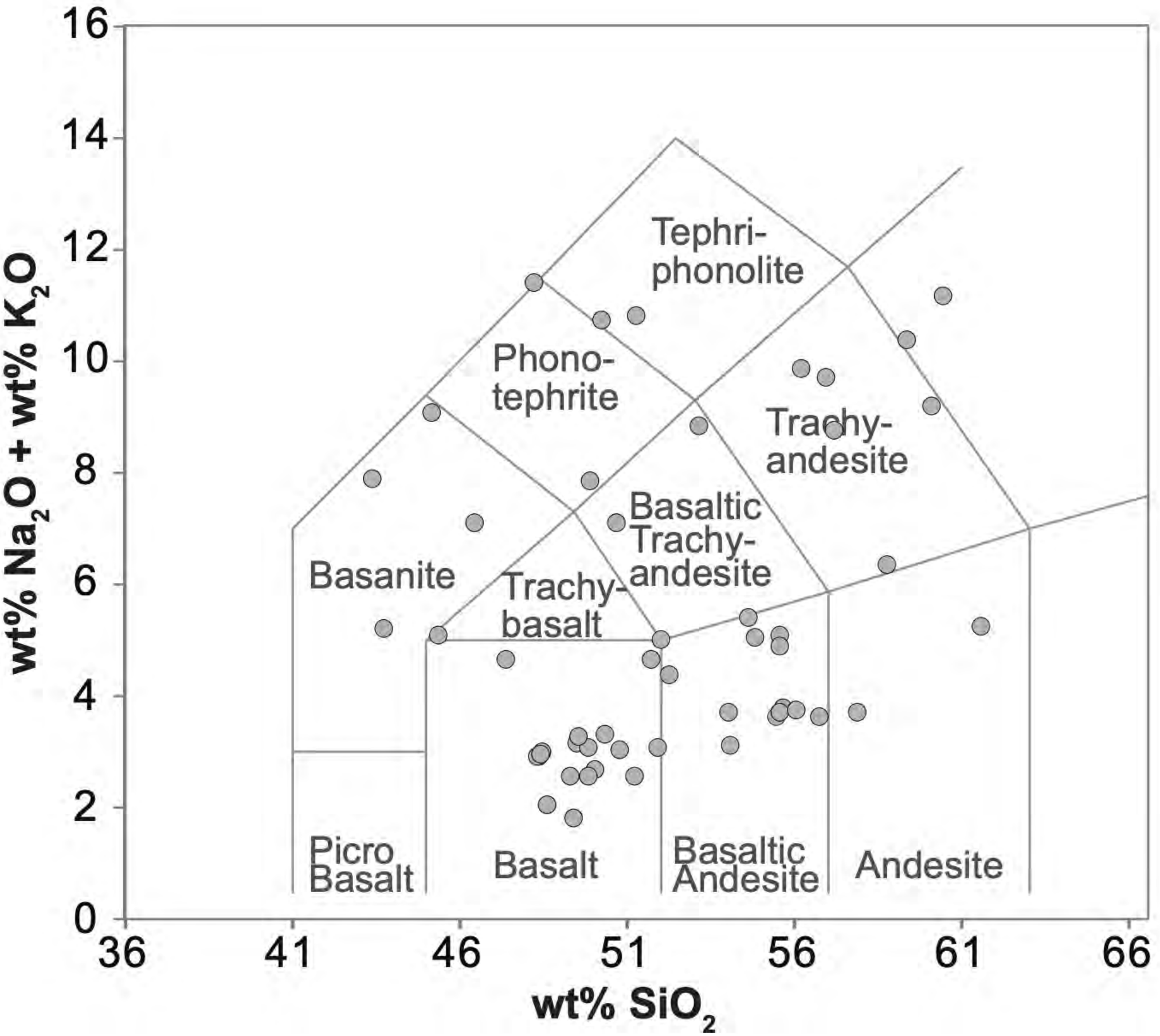
16
14
12
10
8
6
4
2
0
wt% Na2O + wt% K2O
36
41
46
51
56
61
66
wt% SiO2
Tephri-
phonolite
Phono-
tephrite
Trachy-
andesite
Basaltic
Trachy-
andesite
Basanite
Trachy-
basalt
Picro
Basalt
Basalt
Basaltic
Andesite
Andesite

Figure 2

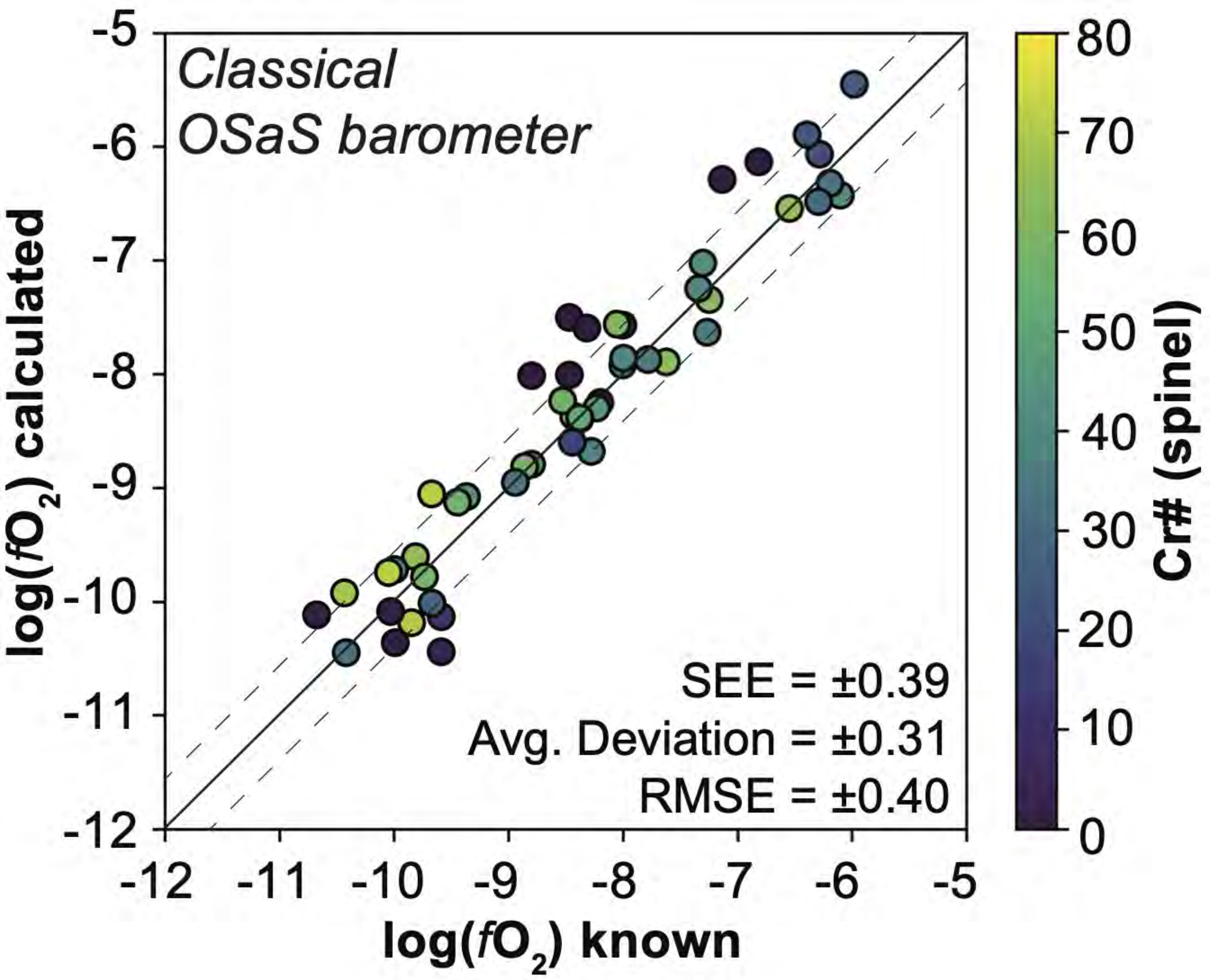
Classical
OSaS barometer
SEE = ±0.39
Avg. Deviation = ±0.31
RMSE = ±0.40
log(fO2) calculated
log(fO2) known
Cr# (spinel)
-5
-6
-7
-8
-9
-10
-11
-12
80
70
60
50
40
30
20
10
0

Figure 3

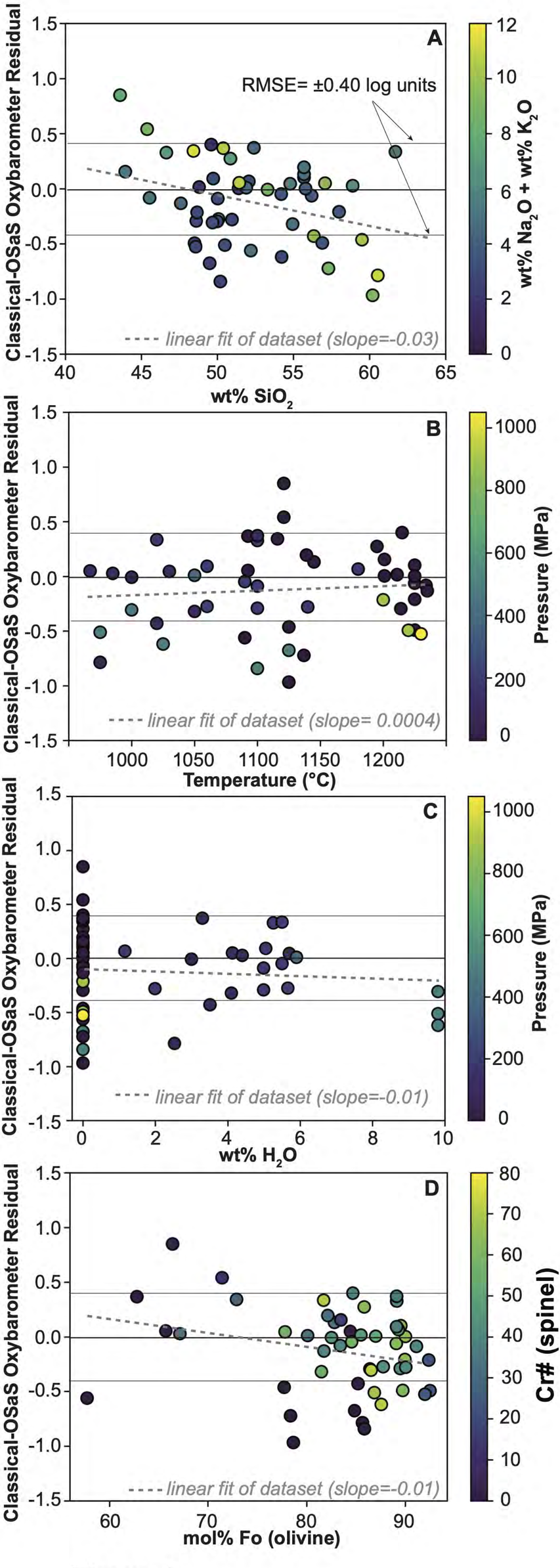
A
RMSE= ±0.40 log units
linear fit of dataset (slope=-0.03)
Classical-OSaS Oxybarometer Residual
wt% SiO2
wt% Na2O + wt% K2O
B
linear fit of dataset (slope= 0.0004)
Temperature (°C)
Pressure (MPa)
C
linear fit of dataset (slope=-0.01)
wt% H2O
D
linear fit of dataset (slope=-0.01)
mol% Fo (olivine)
Cr# (spinel)

Figure 4

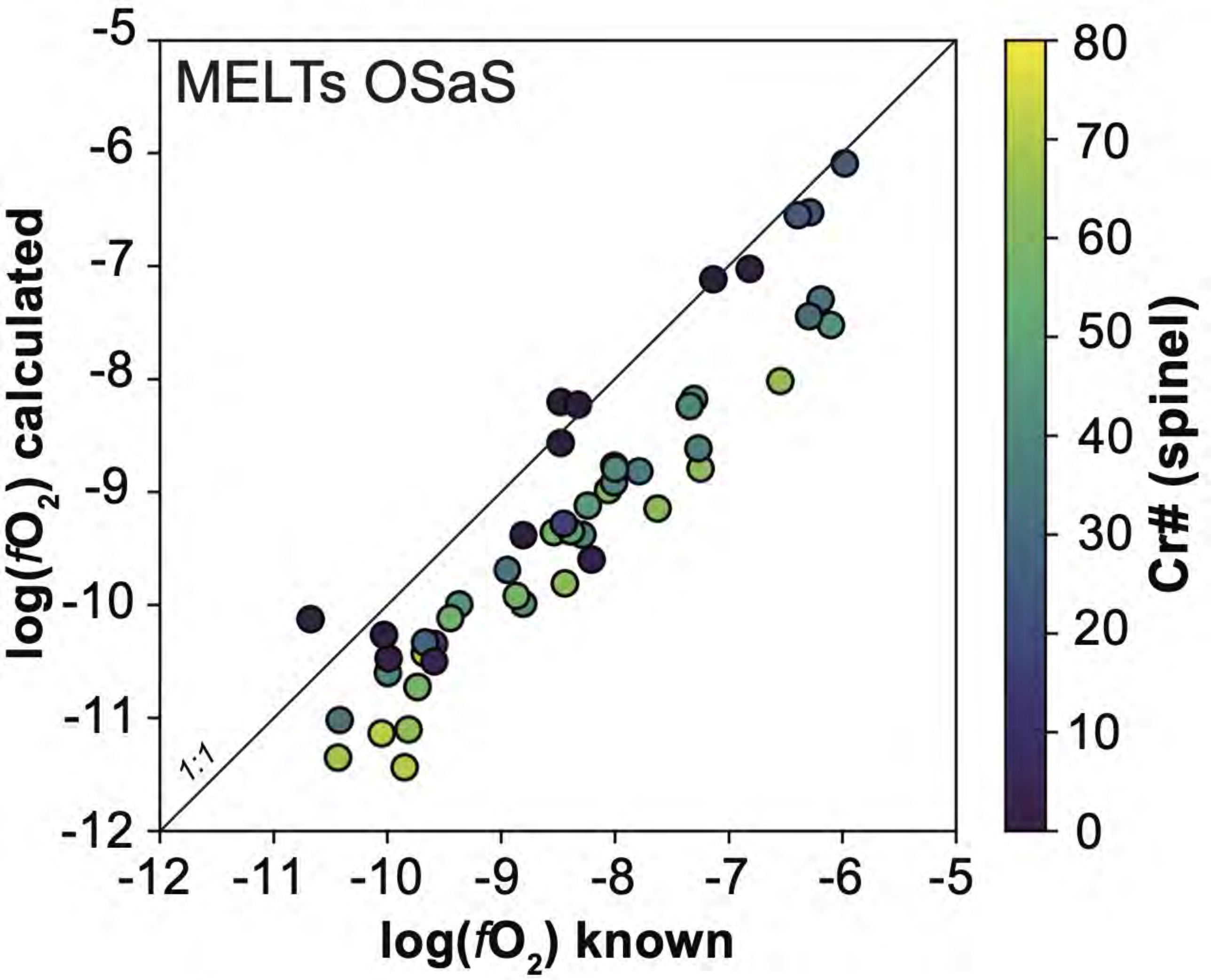
MELTs OSaS
log(fO2) calculated
log(fO2) known
1:1
-5
-6
-7
-8
-9
-10
-11
-12
-12
-11
-10
-9
-8
-7
-6
-5
80
70
60
50
40
30
20
10
0
Cr# (spinel)

Figure 5

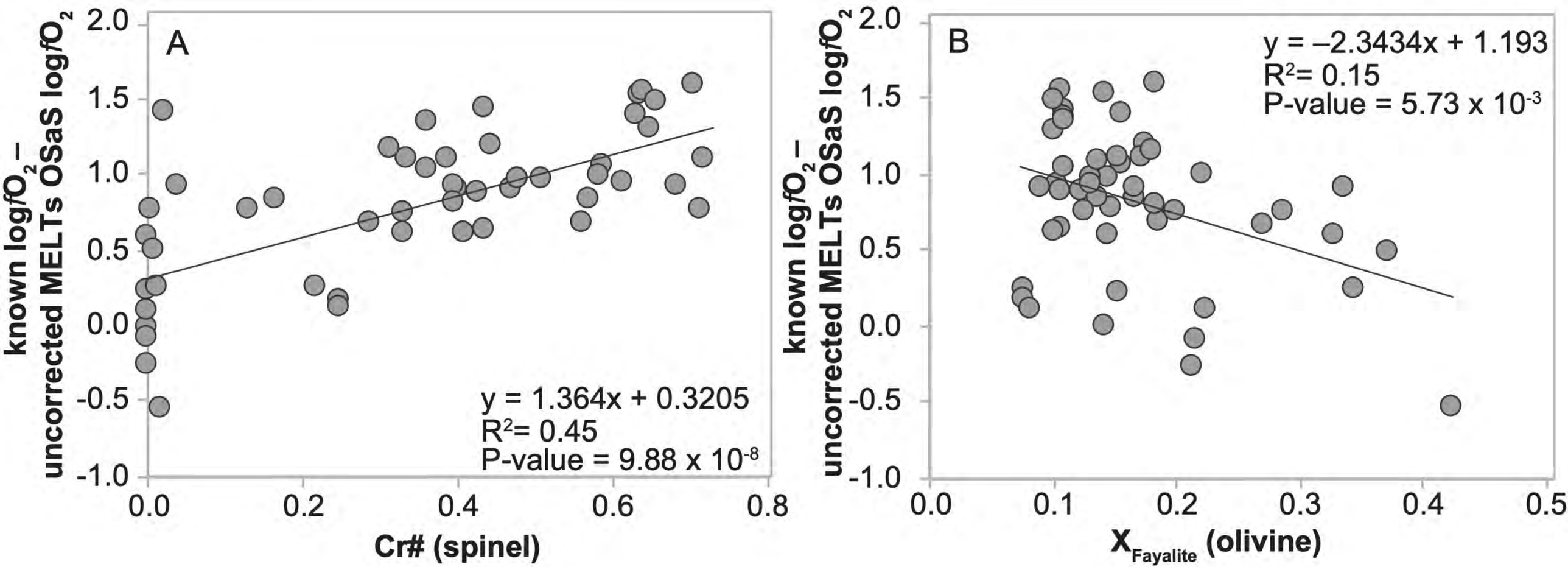
A
y = 1.364x + 0.3205
R²= 0.45
P-value = 9.88 x 10⁻⁸
known logfO_2 – uncorrected MELTs OSaS logfO_2
Cr# (spinel)
B
y = –2.3434x + 1.193
R²= 0.15
P-value = 5.73 x 10⁻³
known logfO_2 – uncorrected MELTs OSaS logfO_2
$X_{Fayalite}$ (olivine)

Figure 6

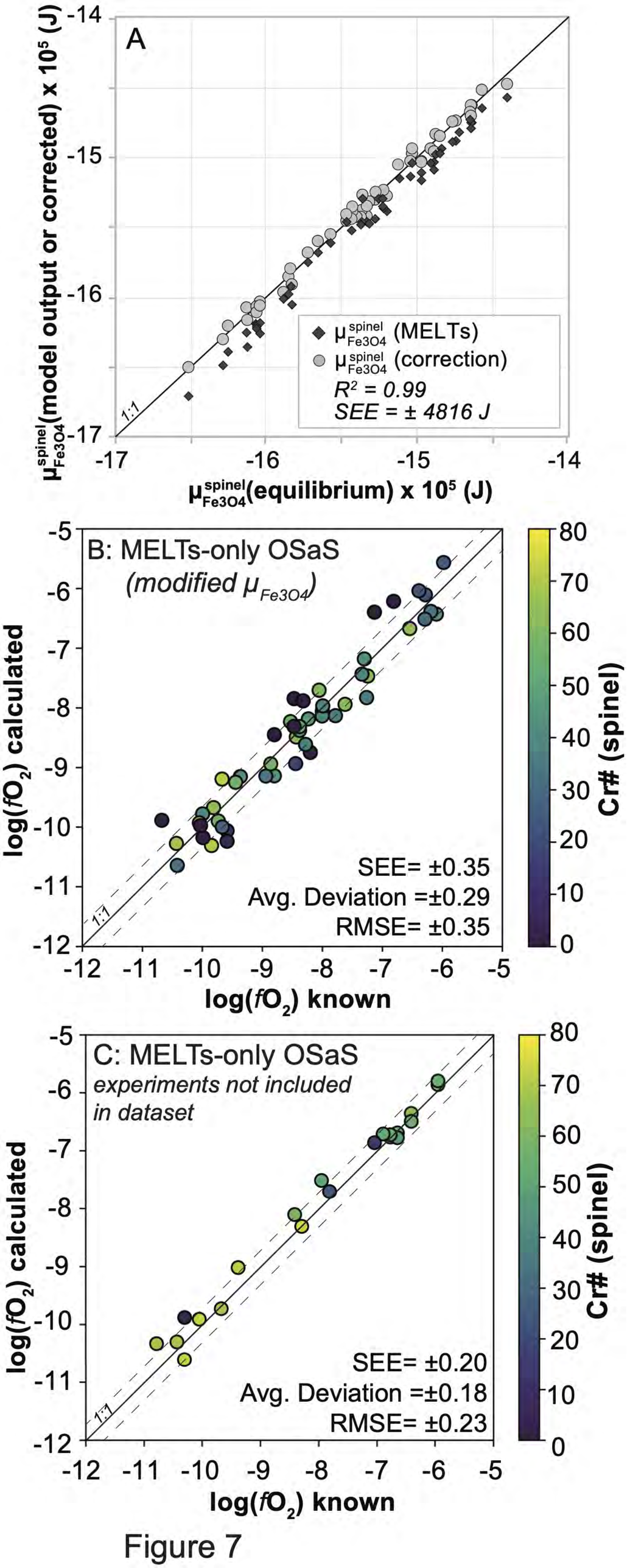
A
μ^{spinel}_{Fe3O4} (MELTs)
μ^{spinel}_{Fe3O4} (correction)
R^2 = 0.99
SEE = ± 4816 J
1:1
μ^{spinel}_{Fe3O4}(model output or corrected) x 10^5 (J)
μ^{spinel}_{Fe3O4}(equilibrium) x 10^5 (J)
B: MELTs-only OSaS
(modified μ_{Fe3O4})
SEE= ±0.35
Avg. Deviation =±0.29
RMSE= ±0.35
log(fO_2) calculated
log(fO_2) known
Cr# (spinel)
C: MELTs-only OSaS
experiments not included
in dataset
SEE= ±0.20
Avg. Deviation =±0.18
RMSE= ±0.23
log(fO_2) calculated
log(fO_2) known
Cr# (spinel)

Figure 7

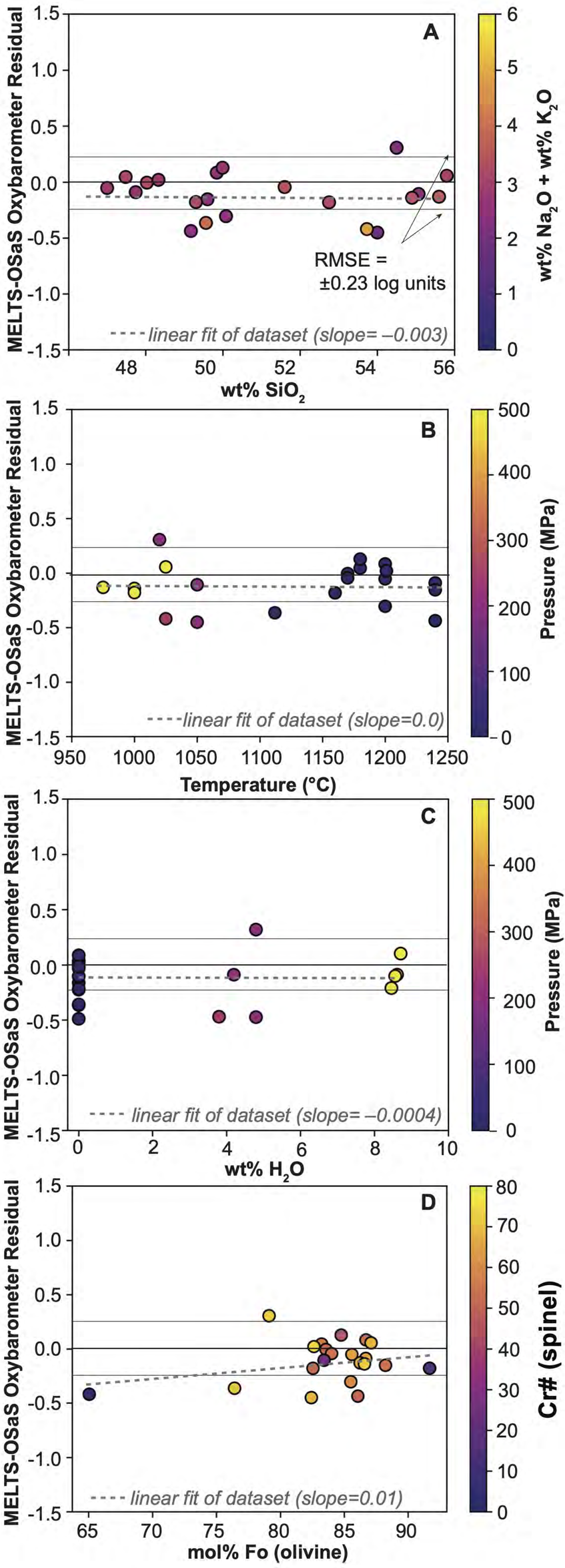
A
MELTS-OSaS Oxybarometer Residual
wt% SiO2
wt% Na2O + wt% K2O
RMSE =
±0.23 log units
linear fit of dataset (slope= –0.003)
B
Temperature (°C)
Pressure (MPa)
linear fit of dataset (slope=0.0)
C
wt% H2O
linear fit of dataset (slope= –0.0004)
D
mol% Fo (olivine)
Cr# (spinel)
linear fit of dataset (slope=0.01)

Figure 8

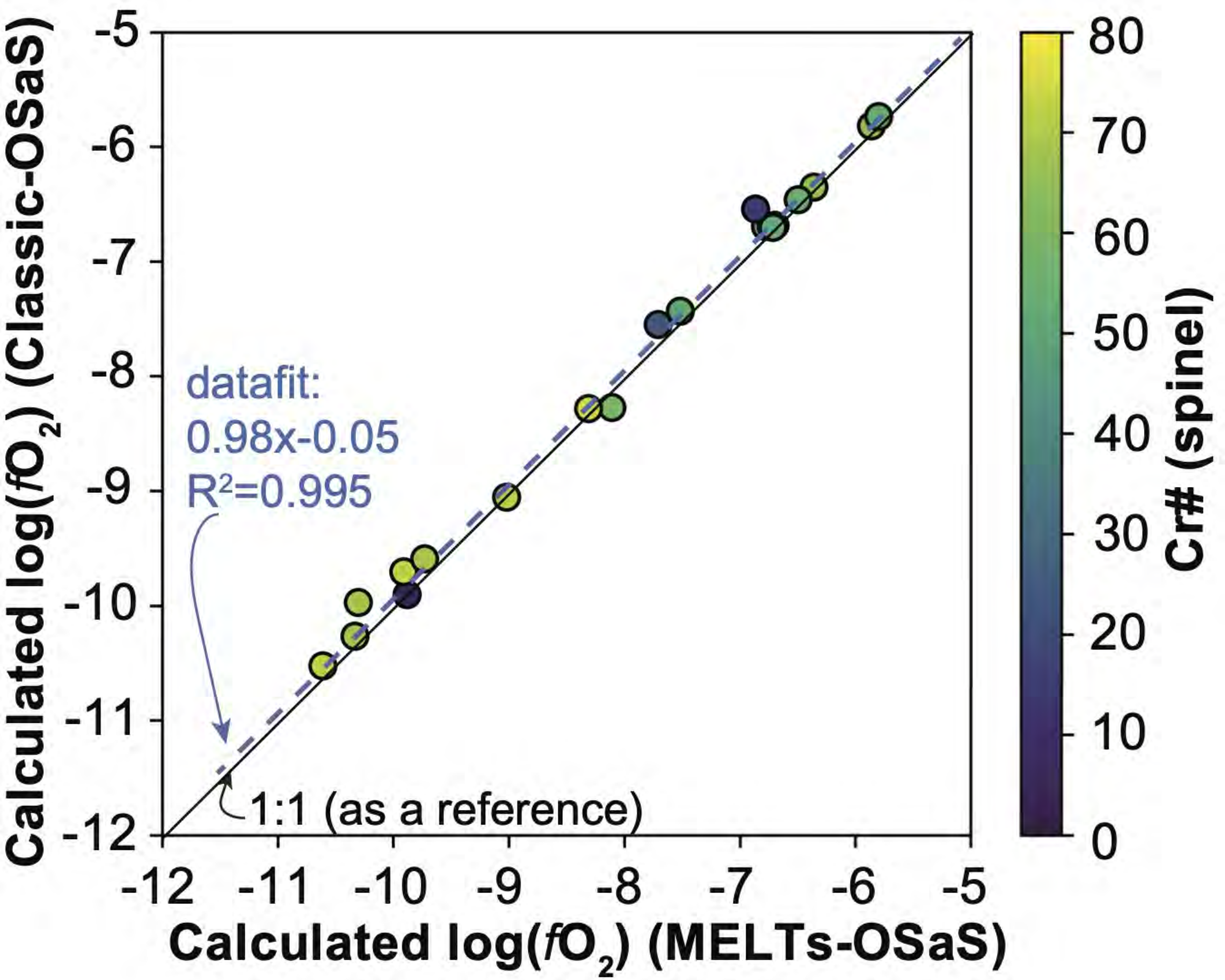
datafit:
0.98x-0.05
R²=0.995
1:1 (as a reference)
Calculated log(fO2) (Classic-OSaS)
Calculated log(fO2) (MELTs-OSaS)
-5
-6
-7
-8
-9
-10
-11
-12
-12
-11
-10
-9
-8
-7
-6
-5
80
70
60
50
40
30
20
10
0
Cr# (spinel)

Figure 9

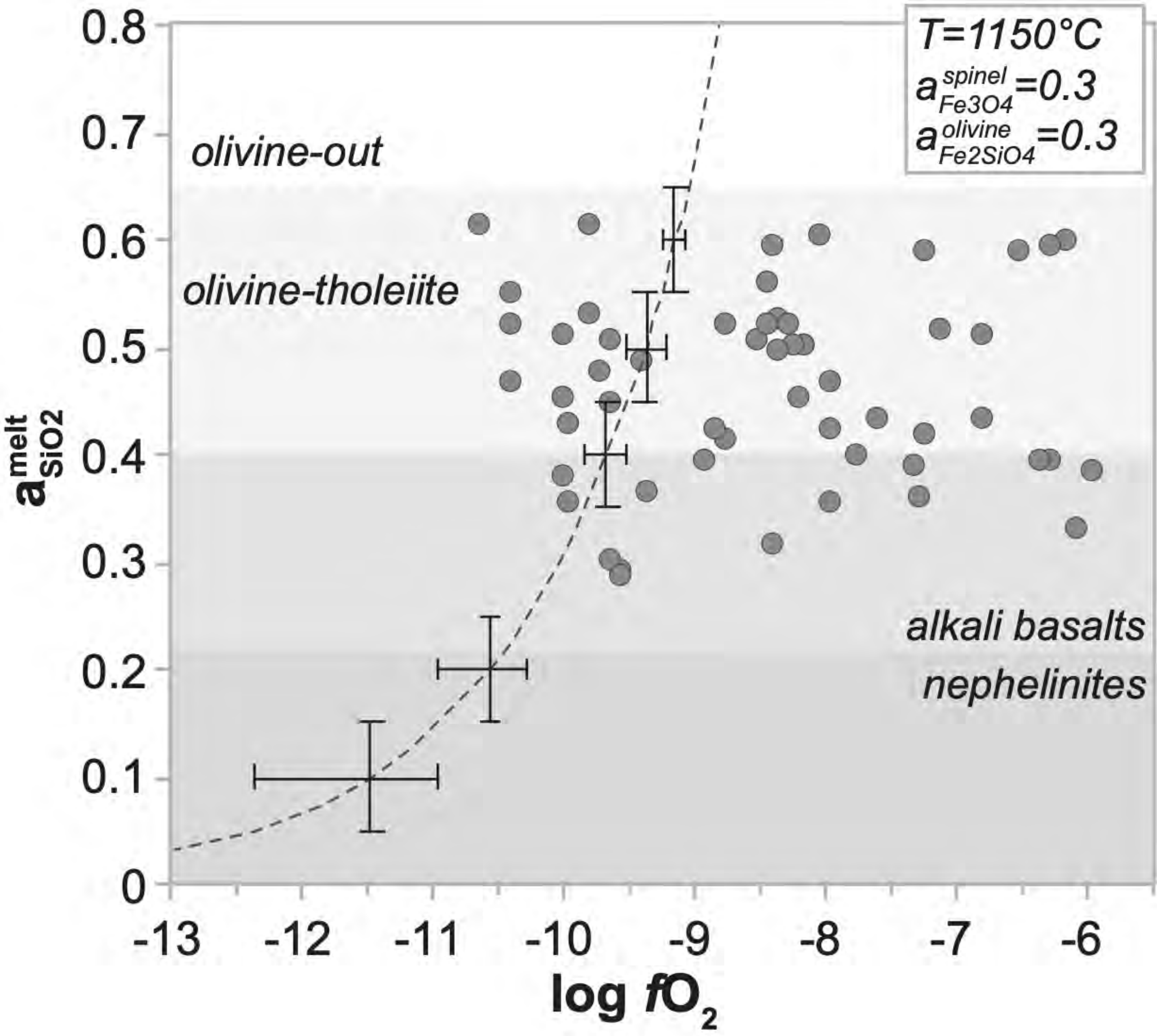
T=1150°C
a^{spinel}_{Fe3O4}=0.3
$a^{olivine}_{Fe2SiO4}$=0.3
olivine-out
olivine-tholeiite
alkali basalts
nephelinites
a^{melt}_{SiO2}
0.8
0.7
0.6
0.5
0.4
0.3
0.2
0.1
0
-13
-12
-11
-10
-9
-8
-7
-6
log fO_2

Figure 10

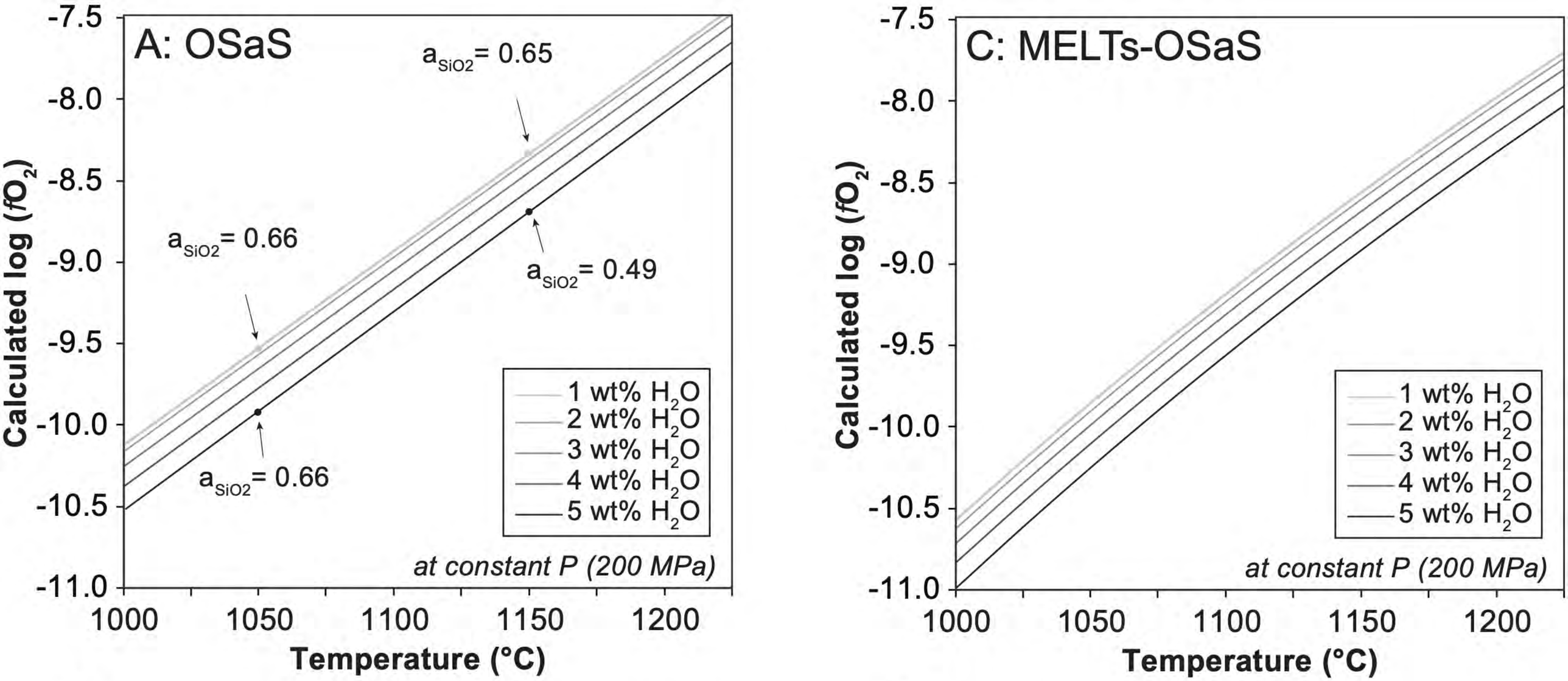
A: OSaS
a_SiO2= 0.65
a_SiO2= 0.66
a_SiO2= 0.49
a_SiO2= 0.66
1 wt% H2O
2 wt% H2O
3 wt% H2O
4 wt% H2O
5 wt% H2O
at constant P (200 MPa)
C: MELTs-OSaS
1 wt% H2O
2 wt% H2O
3 wt% H2O
4 wt% H2O
5 wt% H2O
at constant P (200 MPa)
B: OSaS
ΔrG = 250.0 kJ
ΔrG = 265.6 kJ
ΔrG = 241.2 kJ
ΔrG = 257.4 kJ
100 MPa
200 MPa
300 MPa
400 MPa
500 MPa
at constant H2O (4 wt%)
D: MELTs-OSaS
100 MPa
200 MPa
300 MPa
400 MPa
500 MPa
at constant H2O (4 wt%)
Calculated log (fO2)
Temperature (°C)
-7.5
-8.0
-8.5
-9.0
-9.5
-10.0
-10.5
-11.0
1000
1050
1100
1150
1200

Figure 11

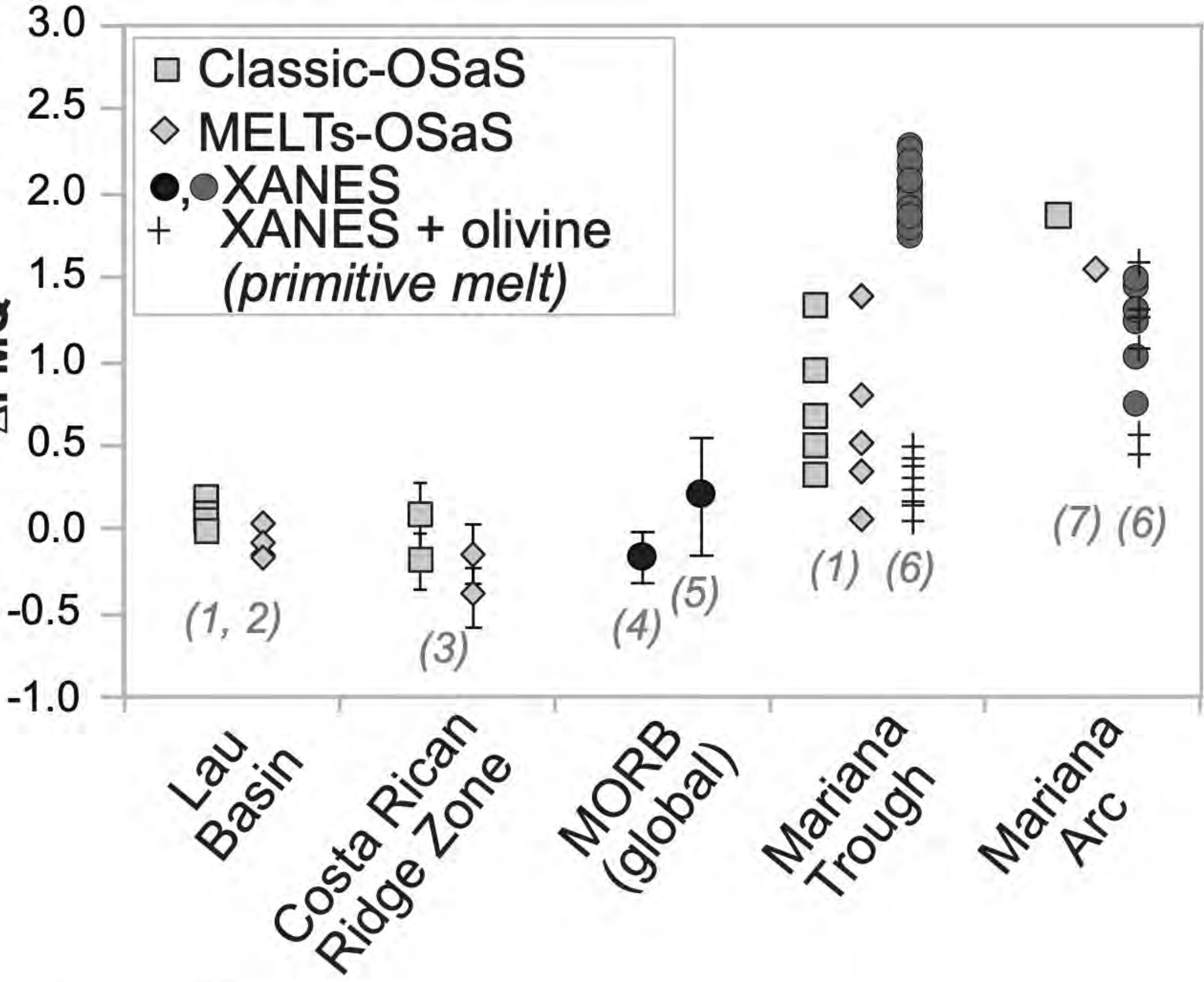
Classic-OSaS
MELTs-OSaS
XANES
XANES + olivine
(primitive melt)
ΔFMQ
3.0
2.5
2.0
1.5
1.0
0.5
0.0
-0.5
-1.0
(1, 2)
(3)
(4)
(5)
(1)
(6)
(7)
(6)
Lau Basin
Costa Rican Ridge Zone
MORB (global)
Mariana Trough
Mariana Arc

Figure 12